

Revisiting Analytical Models of N-Type Symmetric Double-Gate MOSFETs

Rekib Uddin Ahmed and Prabir Saha

Abstract—Nowadays, the endlessly increasing demand for faster and complex integrated circuits (IC) has been fuelled by the scaling of metal-oxide-semiconductor field-effect-transistors (MOSFET) to smaller dimensions. The continued scaling of MOSFETs approaches its physical limits due to short-channel effects (SCE). Double-gate (DG) MOSFET is one of the promising alternatives as it offers better immunity towards SCEs and can be scaled to the shortest channel length. In future, ICs can be designed using DG-CMOS technology for which mathematical models depicting the electrical characteristics of the DG MOSFETs are foremost needed. In this paper, a review on n-type symmetric DG MOSFETs models has been presented based on the analyses of electrostatic potential distribution, threshold voltage, and drain-current models. Mathematical derivations of the device models are described elaborately, and numerical simulations are also carried out to validate the replicability of models.

Index Terms—Analytical modeling, drain-current, n-type DG MOSFETs, potential distribution, review, threshold voltage.

Original Research Paper
DOI: 10.7251/ELS2024015A

I. INTRODUCTION

FOR more than five decades, the semiconductor industries have been successful in providing continuous system performance improvement because of the invention of MOSFETs. Prior to this, bulky vacuum tubes were used for systems, but reliability and heat dissipations were major issues [1]. Therefore, researchers tried to realize the vacuum tube in solid-state for which the surface of semiconductors was studied thoroughly. Lilienfeld first reported the idea of enhancing the surface conductance of a semiconductor by application of electric field in 1930, but it was not successful because of the presence of large densities of surface states

[2]–[3]. The first MOSFET was fabricated in 1960 by Kahng and Atalla [4] on a silicon substrate using an oxide layer (SiO_2) as the gate insulator. Circuits based on single polarity MOSFETs (either p- or n-type) suffered from large static power dissipation, thereby limited the level of integration in a chip. The breakthrough in the level of integration came in 1963 with the invention of complementary metal-oxide-semiconductor (CMOS) [5]. In CMOS technology, both the n- and p-type MOSFETs were constructed side by side on the same substrate, and are connected in series between the supply terminals, so that there is negligible static power dissipation.

The prediction proclaimed by Moore's law has been achieved through scaling of MOSFETs. One of the most important parameters of a MOSFET is its channel length (L), defined as the distance between the source and drain. For a given technology, there is a minimum value of L below which the gate starts to lose control of the drain current (I_{ds}). This is because of the physical limits imposed by non-scalability of silicon energy band-gap (E_g), built-in potential (V_{bi}), short-channel effects (SCEs), and thermal voltage (V_T) [6]. Conventionally, MOSFETs were scaled with a scaling factor s , ($s \approx 0.7$). Scaling by this factor reduces L to $L \times s$, oxide thickness (t_{ox}) to $t_{ox} \times s$, while it increases doping concentration (N_{si}) to N_{si}/s [7]. But this technique cannot be continued in the sub-micron regime, because increasing N_{si} gives rise to mobility degradation of carriers and random dopant fluctuation (RDF) [7,8]. Mobility degradation occurs due to large vertical fields induced by high doping [9]. RDF is a form of process variation due to variation in the implanted dopants which alters the transistor's properties, especially threshold voltage (V_{th}) [10]. So it is utmost important to restore the gate control of the channel without increasing doping concentration of the body. This requirement has led to creating multi-gate (MG) MOSFETs in which body of the device is undoped (or lightly doped). Fig.1 shows some examples of MG MOSFETs where the gate is wrapped around the body from either two or three or four sides.

On decreasing the L , depletion region created by the source and drain encroaches horizontally in the channel, thereby reduces the effective channel length [11]. As the drain-to-source voltage (V_{ds}) increases the depletion region becomes wider. As a result, the channel electrostatics is not only controlled by the gate but also influenced by L and V_{ds} . The observable effects arising due to loss of channel electrostatics controlled by the gate are termed as SCEs. The SCEs include the V_{th} roll-off due to the L reduction, and the drain-induced

Manuscript received 4 October 2019. Received in revised form 18 February 2020. Accepted for publication 5 March 2020.

This work was supported in part by the National Institute of Technology Meghalaya and in part by Visvesvaraya PhD Scheme, Government of India.

Rekib Uddin Ahmed is with the Department of Electronics and Communication Engineering, National Institute of Technology Meghalaya, Shillong 793003, India (e-mail: rekib@nitm.ac.in; phone: +919436594902; fax: +91364-2501113).

Prabir Saha is with the Department of Electronics and Communication Engineering, National Institute of Technology Meghalaya, Shillong 793003, India (e-mail: sahaprabir1@gmail.com; phone: +919485177005; fax: +91364-2501113).

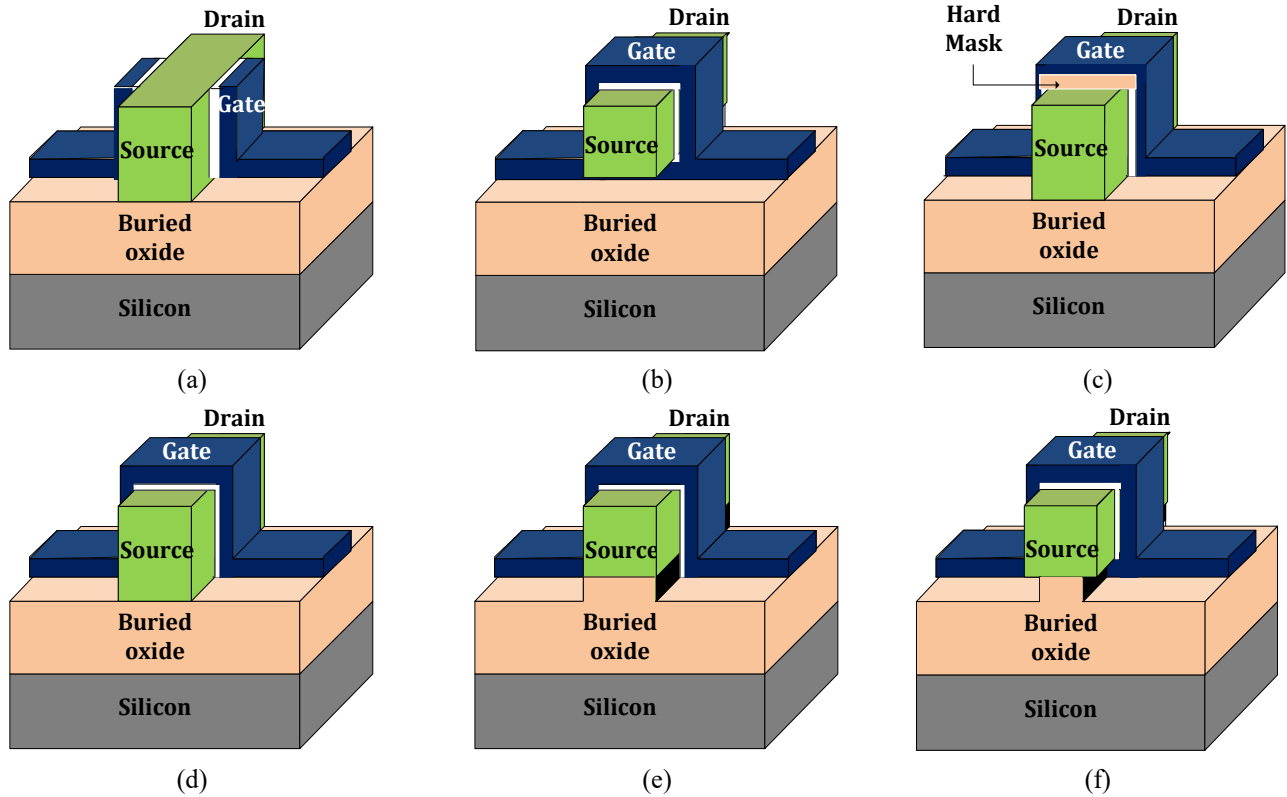


Fig. 1. Different types of MG MOSFETs (a) DG MOSFET, (b) gate-all-around MOSFET, (c) finFET, (d) tri-gate MOSFET, (e) Π -gate MOSFET, (f) Ω -gate MOSFET

barrier lowering (DIBL). These effects cause the V_{th} to decrease upon increasing V_{ds} and also degrades subthreshold slope (SS). Improvement of SCEs by using double-gate architecture was predicted in 1984, which put forward the concept of double-gate (DG) MOSFET [12]. The DG MOSFET is being studied as a key component for future ICs due to its numerous advantages such as excellent gate controllability and improvements in V_{th} roll-off, off-state leakage current and channel length modulation (CLM) effects. The undoped body makes the device immune to RDF, leading to a consistency in the V_{th} from device to device [8]. Due to the undoped body, depletion charge is negligible, which enhances the carrier mobility [13]. The channel inversion takes place throughout the thickness of the body and consequently increases the minority carriers due to which higher current is found [14]. Junction capacitance and mobility degradation are reduced due to which switching speed of the device is improved [13]. Surface roughness scattering due to lower surface electric field is also reduced because of the undoped body [13,14].

All IC designs, digital or analog or mixed-signal, are verified through the use of circuit simulators before being reproduced in real silicon. For any circuit simulator to predict the performance of the ICs based on DG-CMOS technology, it should have accurate models to describe the behaviour of the constituting DG MOSFETs. The device model is a representation of characteristics or conditions in the device in the form of (a) an equation, (b) an equivalent circuit, and (c) a

table, together with the proper reasoning and assumptions. Primary requirements to use a device in the simulators are electrostatic potential distribution (ϕ) model, V_{th} model, and I_{ds} model. Several such models have been reported so far regarding the modeling of n-type DG MOSFETs [15–45]. A brief review on modeling of DG MOSFETs has been presented in [46,47] but the models for short-channel (nanoscale) regimes have not been considered.

Taur [15] developed a ϕ model for long-channel undoped DG MOSFETs where two transcendental equations had to be solved in order to describe the potential distribution in the channel. The need for solving the two equations was removed in the model given by Lu and Taur [16], and thus provided only one equation for potential distribution which in turns required numerical iteration method to get the solution. Hong *et al.* [17] had proposed the ϕ model for a long-channel lightly doped DG MOSFETs by considering the effects of fixed as well as mobile charge carriers. Taur [15] had also given a V_{th} criterion for long-channel DG MOSFETs in which iterative method was used to calculate the V_{th} which was later improved by Chen *et al.* [18] by proposing a new definition for V_{th} . Based on the models [15, 16], Taur *et al.* [19] had given a I_{ds} model for long-channel DG MOSFETs which had three different equations for subthreshold, linear, and saturation regions. Tsormpatzoglou *et al.* [20] presented the ϕ model for short-channel DG MOSFETs based on the parabolic potential approximation method [48] and also presented a semi-analytical model for subthreshold drain

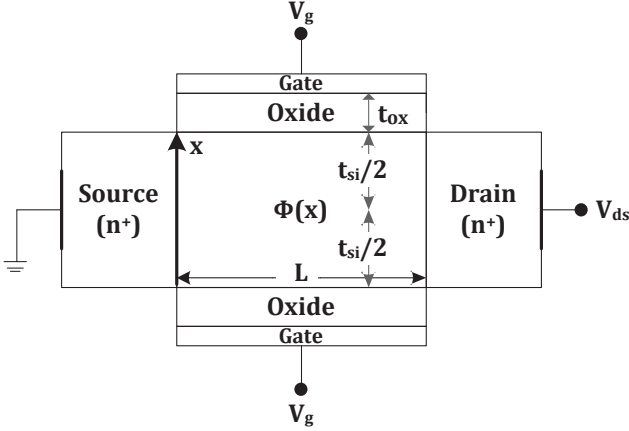


Fig. 2. The cross-sectional view of a long-channel n-type symmetric DG MOSFET along with the geometrical coordinates.

current. Later, the ϕ model [20] was adopted to model the V_{th} in [21] and I_{ds} in [22, 23] for short-channel DG MOSFETs. Recently, Taur and Lin [24] have modified the model [19] by proposing the I_{ds} model for short-channel DG MOSFETs.

In this paper, symmetric n-type DG MOSFET models [15–24] have been reviewed along with their detailed derivations for long and short-channel based on available parameters like ϕ , V_{th} , and I_{ds} . MATLAB code has been presented to demonstrate the semi-analytical modeling given in [20]. At the end, the models [20–23] are adopted to implement n-type DG MOSFET in 30-nm using Verilog-A code [49]. The remaining part of the paper is organized as follows. Section 2 describes the models for long-channel DG MOSFETs in three categories: 1) ϕ models, 2) V_{th} models, and 3) I_{ds} models. Section 3 presents the models for short-channel DG MOSFETs along with MATLAB and Spectre simulations. Section 4 concludes the paper.

II. MODELS FOR LONG CHANNEL DG MOSFETs

A. Electrostatic Potential Models

The electrostatic potential of a long-channel DG MOSFET $\phi(x)$ is one-dimensional (1-D), which is obtained by solving the 1-D Poisson's equation governing the relationship between electric fields and charges. As shown in Fig. 2, $\phi(x)$ is a function of the distance (x) from the gate towards the channel. The $\phi(x)$ models including Taur's [15], and Lu and Taur's [16] for $L = 1\mu\text{m}$ have been considered for the derivation and analysis of V_{th} and I_{ds} models necessary for designing the complete device model for DG MOSFETs.

1) Taur's Model [15]:

The $\phi(x)$ model for an undoped n-type DG MOSFET is derived by considering only the mobile charge density. This is a core model for $L = 1\mu\text{m}$ regime obtained by solving the 1-D Poisson's equation under gradual channel approximation (GCA) [50] assuming Boltzmann statistics for mobile charges. The GCA assumes that variation in lateral electric field

much less than the variation in the vertical electric field (along x) so that the 2-D Poisson's equation reduces to 1-D [51]. Finally, the $\phi(x)$ model is expressed as:

$$\phi(x) = \phi_0 - 2V_T \ln \left[\cos \left(\sqrt{\frac{qn_i}{2\epsilon_{si}V_T}} e^{\frac{\phi_0}{2V_T}x} \right) \right] \quad (1)$$

where $\phi_0 \equiv \phi(x=0)$, V_T is the thermal voltage, n_i is the intrinsic charge density, and ϵ_{si} is the dielectric permittivity of silicon. $\phi(x)$ is also defined as the amount of band bending or position of intrinsic potential at x [51]. A similar form of solution (1) was earlier given by Hauser and Littlejohn [52]. Derivation of the model (1) is as follows.

The 1-D Poisson's equation for the silicon region considering only mobile charge density is expressed as:

$$\frac{d^2\phi(x)}{dx^2} = \frac{q}{\epsilon_{si}} n_i e^{\frac{q\phi(x)}{k_bT}}, \quad (2)$$

where q is the elementary charge, k_b is the Boltzmann constant, and T is the temperature. By interpreting in terms of $d\phi$ and integrating both sides, (2) can be rewritten as:

$$\int_0^{\phi(x)} \frac{d\phi}{dx} \left(\frac{d\phi}{dx} \right) d \left(\frac{d\phi}{dx} \right) = \int_{\phi_0}^{\phi(x)} \frac{q}{\epsilon_{si}} n_i e^{\frac{q\phi}{k_bT}} d\phi. \quad (3)$$

On solving (3):

$$\left(\frac{d\phi}{dx} \right) = \sqrt{\frac{2k_bTn_i}{\epsilon_{si}} \left(e^{\frac{q\phi(x)}{k_bT}} - e^{\frac{q\phi_0}{k_bT}} \right)}. \quad (4)$$

Integrating both sides of (4):

$$\int_{\phi_0}^{\phi(x)} \frac{d\phi}{\sqrt{\frac{2k_bTn_i}{\epsilon_{si}} \left(e^{\frac{q\phi(x)}{k_bT}} - e^{\frac{q\phi_0}{k_bT}} \right)}} = \int_0^x dx. \quad (5)$$

Considering $e^{\frac{q\phi(x)}{k_bT}} - e^{\frac{q\phi_0}{k_bT}} = t$ will imply:

$$e^{\frac{q\phi(x)}{k_bT}} = t + e^{\frac{q\phi_0}{k_bT}}. \quad (6)$$

Differentiating (6) with respect to ϕ :

$$\frac{d}{d\phi} e^{\frac{q\phi}{k_bT}} = \frac{dt}{d\phi} = \frac{q}{k_bT} e^{\frac{q\phi}{k_bT}}. \quad (7)$$

Rearranging the terms of (7):

$$d\phi = \frac{k_bT}{q} e^{-\frac{q\phi}{k_bT}} dt = \frac{k_bT}{q} \frac{dt}{\left(t + e^{\frac{q\phi_0}{k_bT}} \right)}. \quad (8)$$

Substituting (8) and (6) in (5) will yield:

$$\int_0^t \frac{dt}{\sqrt{t} \left(t + e^{\frac{q\phi_0}{k_bT}} \right)} = \sqrt{\frac{2q^2n_i}{\epsilon_{si}k_bT}} \int_0^x dx. \quad (9)$$

Considering $\sqrt{t} = z$ in (9) and substituting $dt = 2zdz$ in (9) will imply:

$$\int \frac{2dz}{\left(z^2 + e^{\frac{q\phi_0}{k_bT}}\right)} = \sqrt{\frac{2q^2n_i}{\varepsilon_{si}k_bT}} \chi. \quad (10)$$

$$\frac{2}{\frac{q\phi_0}{e^{2k_bT}}} \tan^{-1}\left(\frac{z}{\frac{q\phi_0}{e^{2k_bT}}}\right) = \sqrt{\frac{2q^2n_i}{\varepsilon_{si}k_bT}} \chi. \quad (11)$$

$$z = e^{\frac{q\phi_0}{2k_bT}} \tan\left(\sqrt{\frac{q^2n_i}{2\varepsilon_{si}k_bT}} e^{\frac{q\phi_0}{2k_bT}} \chi\right). \quad (12)$$

$$t = e^{\frac{q\phi_0}{k_bT}} \tan^2\left(\sqrt{\frac{q^2n_i}{2\varepsilon_{si}k_bT}} e^{\frac{q\phi_0}{2k_bT}} \chi\right). \quad (13)$$

$$e^{\frac{q\phi(x)}{k_bT}} - e^{\frac{q\phi_0}{k_bT}} = e^{\frac{q\phi_0}{k_bT}} \tan^2\left(\sqrt{\frac{q^2n_i}{2\varepsilon_{si}k_bT}} e^{\frac{q\phi_0}{2k_bT}} \chi\right). \quad (14)$$

$$e^{\frac{q\phi(x)}{k_bT}} = e^{\frac{q\phi_0}{k_bT}} \left[1 + \tan^2\left(\sqrt{\frac{q^2n_i}{2\varepsilon_{si}k_bT}} e^{\frac{q\phi_0}{2k_bT}} \chi\right)\right]. \quad (15)$$

Rearranging terms of (15) :

$$e^{\frac{q(\phi(x)-\phi_0)}{k_bT}} = \sec^2\left(\sqrt{\frac{q^2n_i}{2\varepsilon_{si}k_bT}} e^{\frac{q\phi_0}{2k_bT}} \chi\right). \quad (16)$$

$$\frac{q(\phi(x)-\phi_0)}{k_bT} = 2 \ln\left(\sec\left[\sqrt{\frac{q^2n_i}{2\varepsilon_{si}k_bT}} e^{\frac{q\phi_0}{2k_bT}} \chi\right]\right). \quad (17)$$

$$\phi(x) = \phi_0 - \frac{2k_bT}{q} \ln\left[\cos\left(\sqrt{\frac{q^2n_i}{2\varepsilon_{si}k_bT}} e^{\frac{q\phi_0}{2k_bT}} \chi\right)\right]. \quad (18)$$

Since, $\frac{k_bT}{q} = V_T$ so substituting V_T will finally give the $\phi(x)$ model (1).

2) Lu and Taur Model [16]:

This model extended the model [15] by considering quasi-Fermi potential (ϕ_F) in (1). ϕ_F is the potential difference between electron and hole quasi-Fermi levels along the channel $\phi_F = \varphi_{Fn} - \varphi_{Fp}$. In short, ϕ_F is the voltage drop in the channel whose value ranges from $\phi_F = 0$ at source to V_{ds} at the drain. Considering this ϕ_F in equation (2), the 1-D Poisson's equation is expressed as:

$$\frac{d^2\phi(x)}{dx^2} = \frac{q}{\varepsilon_{si}} n_i e^{\frac{q(\phi(x)-\phi_F)}{k_bT}}. \quad (19)$$

Inclusion of the ϕ_F will transform the model (18) as:

$$\phi(x) - \phi_F = \phi_0 - \phi_F - \frac{2k_bT}{q} \ln\left[\cos\left(\sqrt{\frac{q^2n_i}{2\varepsilon_{si}k_bT}} e^{\frac{q(\phi_0-\phi_F)}{2k_bT}} \chi\right)\right]. \quad (20)$$

A parameter β has been introduced, which is a function of ϕ_F but independent of x [53].

$$\beta = \frac{t_{si}}{2} \sqrt{\frac{q^2n_i}{2\varepsilon_{si}k_bT}} e^{\frac{q(\phi_0-\phi_F)}{2k_bT}}. \quad (21)$$

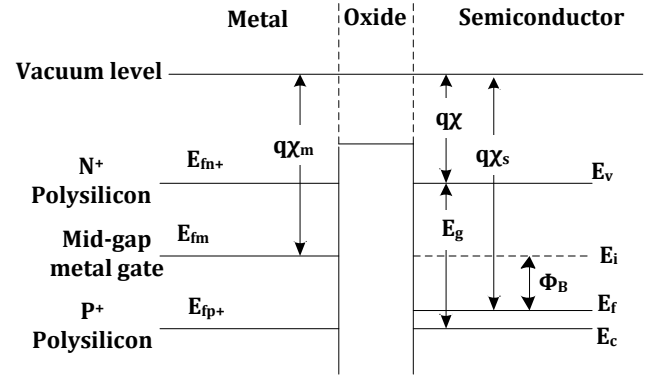


Fig. 3. Fermi-energy levels (E_{fm+} , E_{fm} , and E_{fm-}) of n^+ , p^+ polysilicon, and mid-gap metal gate. E_g is the energy band-gap of semiconductor. χ is the electron-affinity of the semiconductor. χ_m and χ_s are the work-functions of mid-gap metal gate and semiconductor, respectively.

Rearranging the terms in (21):

$$\phi_0 - \phi_F = \frac{2k_bT}{q} \ln\left[\frac{2\beta}{t_{si}} \sqrt{\frac{2\varepsilon_{si}k_bT}{q^2n_i}}\right]. \quad (22)$$

On substituting (22) in (20) will yield:

$$\phi(x) = \phi_F - \frac{2k_bT}{q} \ln\left[\frac{t_{si}}{2\beta} \sqrt{\frac{q^2n_i}{2\varepsilon_{si}k_bT}} \cos\left(\frac{2\beta}{t_{si}} \chi\right)\right]. \quad (23)$$

The surface potential at $x = t_{si}/2$ [Fig. 2] is expressed as:

$$\phi_s \equiv \phi\left(x = \frac{t_{si}}{2}\right) = \phi_F - \frac{2k_bT}{q} \ln\left[\frac{t_{si}}{2\beta} \sqrt{\frac{q^2n_i}{2\varepsilon_{si}k_bT}} \cos\left(\frac{2\beta}{t_{si}} \chi\right)\right]. \quad (24)$$

Equation (23) is the $\phi(x)$ model given by Lu and Taur which has been taken by many research groups [22–23], [33–34] to model the short-channel DG MOSFET characteristics. Applying boundary condition at silicon-oxide interface:

$$\varepsilon_{ox} \frac{V_g - \Delta\chi_{ms} - \phi_s}{t_{ox}} = \varepsilon_{si} \frac{d\phi}{dx} \Big|_{x=\frac{t_{si}}{2}}, \quad (25)$$

where V_g is the applied gate voltage and $\Delta\chi_{ms}$ is the work-function difference between the gates and the silicon as shown in Fig. 3. In case of undoped body $\Delta\chi_{ms} = 0$ for mid-gap metal gate, $-E_g/2q$ for n^+ polysilicon, and $E_g/2q$ for p^+ polysilicon. Differentiating (23) with respect to x :

$$\frac{d\phi}{dx} = \frac{-2V_T \frac{t_{si}}{2\beta} \sqrt{\frac{q^2n_i}{2\varepsilon_{si}k_bT}} \left[-\sin\frac{2\beta}{t_{si}} \chi\right] \frac{2\beta}{t_{si}}}{\frac{t_{si}}{2\beta} \sqrt{\frac{q^2n_i}{2\varepsilon_{si}k_bT}} \cos\frac{2\beta}{t_{si}} \chi} = 2V_T \frac{2\beta}{t_{si}} \tan\left(\frac{2\beta}{t_{si}} \chi\right). \quad (26)$$

Substituting (24) and (26) in (25):

$$\frac{V_g - \Delta\chi_{ms} - \phi_F}{2V_T} - \ln \left[\frac{2}{t_{si}} \sqrt{\frac{2\varepsilon_{si}k_bT}{q^2n_i}} \right] = \ln \beta - \ln \cos \beta + 2r\beta \tan \beta, \quad (27)$$

with $r = \frac{\varepsilon_{si}t_{ox}}{\varepsilon_{ox}t_{si}}$. The value of β has to be calculated from (27) using numerical iterations like Newton-Raphson method [54]. Numerical iteration and algorithms increase the computation time. Fast and efficient method has to be adopted to make the model suitable for circuit simulation. Yu *et al.* [25] developed a computation method which eliminated the need for numerical iterations.

3) Hong *et al.* [17]:

The $\phi(x)$ models of DG MOSFETs developed in [15, 16] are valid for the undoped silicon body. The work has been extended by Hong *et al.* [17] by proposed the $\phi(x)$ model for the lightly doped silicon body with spatially varying doping profiles. The $\phi(x)$ model derived through solving the 1-D Poisson's equation considering both the fixed and mobile charge density.

$$\frac{d^2\phi(x)}{dx^2} = \frac{qn_i^2}{\varepsilon_{si}N_{si}} e^{\frac{q(\phi(x)-\phi_F)}{k_bT}} + \frac{qN_{si}(x)}{\varepsilon_{si}}, \quad (28)$$

where $N_{si}(x)$ is the spatially varying doping distribution in the silicon body (can be continuous or discrete). Consideration of fixed and mobile charge density in a lightly-doped silicon body is required from the accuracy point of view [31,32]. Because, the effect of mobile charge density cannot neglected in the above subthreshold regime [33] and its inclusion in Poisson's equation enhances the model accuracy [55]. Substituting $\frac{qN_{si}(x)}{\varepsilon_{si}} = \frac{d^2g(x)}{dx^2}$, (28) can be written as:

$$\phi(x) = \frac{k_bT}{q}Z(x) + \phi_F + g(x). \quad (29)$$

Differentiating (29) twice with respect to x :

$$\frac{d^2\phi(x)}{dx^2} = \frac{k_bT}{q} \frac{d^2Z(x)}{dx^2} + \frac{d^2g(x)}{dx^2}. \quad (30)$$

Substituting (30) in (28) will yield:

$$\frac{k_bT}{q} \frac{d^2Z(x)}{dx^2} + \frac{d^2g(x)}{dx^2} = \frac{qn_i^2}{\varepsilon_{si}N_{si}} e^{\frac{q}{k_bT}(\frac{k_bT}{q}Z(x)+g(x))} + \frac{qN_{si}(x)}{\varepsilon_{si}},$$

which on solving will yield:

$$\frac{d^2Z(x)}{dx^2} = \frac{q^2n_i^2}{k_bT\varepsilon_{si}} e^{Z(x)} \frac{e^{\frac{q}{k_bT}g(x)}}{N_{si}}. \quad (31)$$

Substituting $\text{Exp} \left[\frac{q}{k_bT}g(x) \right] / N_{si} = f(x)$ and $\frac{q^2n_i^2}{k_bT\varepsilon_{si}} = \xi$, (31) is re-written as:

$$\frac{d^2Z(x)}{dx^2} = \xi e^{Z(x)} f(x). \quad (32)$$

The terms ξ and $f(x)$ in (32) contain the effect of nonlinear coupling between the mobile and fixed charge densities. Presence of the $f(x)$ makes this modeling scheme unique from the exiting $\phi(x)$ model [56] for the DG MOSFET. In order to

derive the analytical solution for $\phi(x)$, the (32) (in Cartesian coordinate) is transformed into the cylindrical coordinate.

$$\frac{d^2Z_c(\tau)}{d\tau^2} + \frac{1}{\tau} \frac{dZ_c(\tau)}{d\tau} = \xi e^{Z_c(\tau)} F(\tau), \quad (33)$$

where $Z_c(\tau) = Z(x) - 2$, $\ln \tau = x$, and $F(\tau) = f(\ln \tau)$. In order to solve (32), two new variables are introduced: $\beta = \tau \frac{dZ_c}{d\tau}$ and $\eta = \tau^2 F(\tau) e^{Z_c(\tau)}$. Differentiating β with respect to τ will yield:

$$\frac{d\beta}{d\tau} = \frac{dZ_c(\tau)}{d\tau} + \tau \frac{d^2Z_c(\tau)}{d\tau^2}. \quad (34)$$

Substituting $\frac{d^2Z_c(\tau)}{d\tau^2}$ from (34) in (33):

$$\frac{d\beta}{d\tau} = \tau \xi e^{Z_c(\tau)} F(\tau). \quad (35)$$

Differentiating η with respect to τ will yield:

$$\frac{d\eta}{d\tau} = 2\tau F(\tau) e^{Z_c(\tau)} + \tau^2 F'(\tau) e^{Z_c(\tau)} + \tau^2 F(\tau) e^{Z_c(\tau)} \frac{dZ_c}{d\tau}. \quad (36)$$

Substituting $\beta = \tau \frac{dZ_c}{d\tau}$ and rearranging the terms of (36):

$$\tau e^{Z_c(\tau)} F(\tau) = \frac{d\eta}{d\tau} \frac{1}{\left[2 + \tau \frac{F'(\tau)}{F(\tau)} + \beta \right]}. \quad (37)$$

On substituting (37) in (35) will further transform the (33) to:

$$d\beta[\beta + p(\tau)] = \xi d\eta, \quad (38)$$

where $p(\tau) = 2 + \tau \frac{F'(\tau)}{F(\tau)}$ is the spatial function related to the doping profile, i.e. whether continuous or discrete doping. Equation (38) is integrated to obtain:

$$\frac{\beta^2}{2} + p(\tau)\beta - h = \xi\eta, \quad (39)$$

where $h = -\xi\eta_0 - 2p + 2$ is an integration constant to be determined from boundary conditions. Substituting $\beta = \tau \frac{dZ_c}{d\tau}$ and $\eta = \tau^2 F(\tau) e^{Z_c(\tau)}$ in (39) and using (32) will yield :

$$\frac{d^2Z_c(\tau)}{d\tau^2} - \frac{[p(\tau)-1]}{\tau} \frac{dZ_c(\tau)}{d\tau} - \frac{1}{2} \left(\frac{dZ_c(\tau)}{d\tau} \right)^2 + \frac{h}{\tau^2} = 0. \quad (40)$$

On solving (40), the general solution of 1-D Poisson's equation can be readily obtained as:

$$Z_c = -p \ln \tau + A - 2 \ln \left| \cos \left(\frac{1}{2} \sqrt{-(p-2)^2 - 2h} \ln \tau - B \sqrt{-(p-2)^2 - 2h} \right) \right|, \quad (41)$$

where A and B are the integration constants. Here the $\beta(\tau)$ is approximated as:

$$\beta(\tau) = -p + \sqrt{-(p-2)^2 - 2h} \quad (42)$$

$$\tan \left\{ \frac{1}{2} \sqrt{-(p-2)^2 - 2h} \left(\ln \tau - \frac{t_{si}}{2} \right) + \tan^{-1} \left[\frac{\beta_s + p}{\sqrt{-(p-2)^2 - 2h}} \right] \right\},$$

where β_s is value of $\beta(\tau)$ at the surface ($\tau = e^{\frac{t_{si}}{2}}$) and can be approximated from the relation:

$$\frac{\beta_s^2}{2} - \frac{\beta_0^2}{2} + M = \xi(\eta_s - \eta_0), \quad (43)$$

where β_0 is value of $\beta(\tau)$ at the center of the silicon body ($\tau = 1$). For the symmetric DG MOSFETs, $\beta_0 = dZ_C/d\tau|_{\tau=1} = -2$ is considered. $M = \int_1^{e^{\frac{t_{si}}{2}}} \left[p(\tau) \frac{d\beta}{d\tau} \right] d\tau$ is an integral to be solved. η_0 is calculated from the relation:

$$\eta_0 = \frac{c(\beta_s + 2)}{\xi \left[1 + \frac{(\beta_s + 2)}{(\beta_c + 2)} \right]}, \quad (44)$$

where β_c is the value of β_s when η_0 reaches its saturation value η_{0sat} whose value is given by: $\beta_c = \frac{\xi \eta_{0sat}}{c-2}$. The parameters c , η_{0sat} are expressed as:

$$c = \frac{\xi \varepsilon_{si} k_b T F(1)}{q \theta_s}, \quad \text{with } \theta_s = \int_0^{\frac{t_{si}}{2}} \frac{q N_{si} x^2}{\varepsilon_{si}^2} e^{\frac{q N_{si} x^2}{k_b T}} dx, \quad (45)$$

$$\eta_{0sat} = 1 \times F(1) \times e^{Z_{Csat}}$$

$$\text{with } Z_{Csat} \approx 2 \ln \left(\frac{N_{si}}{n_i} \right) - \ln[1 - e^{-2\alpha}] - \alpha + 1.6$$

$$\text{where } \alpha = \frac{q^2 N_{si} t_{si}^2}{8 \varepsilon_{si} k_b T}.$$

The potential distribution characteristics obtained from the model (41) is able show the variation of electrostatic potential with respect to the V_g from weak to strong inversion regime.

B. Threshold Voltage Models

The V_{th} of conventional bulk MOSFET is defined as the V_g at which the minimum surface potential value $\phi_{s,min}$ reaches twice the bulk potential ϕ_B [51]. ϕ_B is the potential difference between the Fermi-level (E_f) and the intrinsic level (E_i) of the semiconductor [Fig. 3]. The ϕ_B definition of V_{th} does not work for DG MOSFETs, where the doping concentration is $N_{si} \leq 10^{16} \text{ cm}^{-3}$ [18,33].

1) Taur's Model [15]:

The threshold criterion for long-channel DG MOSFETs given by Taur [15] used iterative method to calculate the V_{th} by extrapolating the linear dependency of inversion charge sheet density Q_{inv} with V_g using the relation: $Q_{inv} = 2C_{ox}(V_g - \Delta\chi_{ms} - \phi_s)$. Where $\phi_s \equiv \phi(x = t_{si}/2)$ is the surface potential. The threshold condition is given by: $V_{th} = \Delta\chi_{ms} - \phi_s$. The detailed derivation of the model is as follows.

The effective gate voltage at the silicon-oxide interface is expressed as:

$$V_{gt} = V_g - \Delta\chi_{ms} - \phi_s. \quad (46)$$

Applying boundary condition at the silicon-oxide interface:

$$\varepsilon_{ox} \frac{V_g - \Delta\chi_{ms} - \phi_s}{t_{ox}} = \varepsilon_{si} \frac{d\phi}{dx} \Big|_{x=t_{si}/2}. \quad (47)$$

Substituting $\frac{d\phi}{dx} \Big|_{x=t_{si}/2}$ from (4) in (47):

$$\varepsilon_{ox} \frac{V_g - \Delta\chi_{ms} - \phi_s}{t_{ox}} = \sqrt{2\varepsilon_{si} k_b T n_i \left(e^{\frac{q\phi_s}{k_b T}} - e^{\frac{q\phi_0}{k_b T}} \right)}. \quad (48)$$

ϕ_s is increased with increase in V_g , whereas the center potential ϕ_0 attains a constant value. For greater value of V_g (more than threshold), the term ϕ_0 in (48) can be neglected which will imply:

$$\varepsilon_{ox} \frac{V_g - \Delta\chi_{ms} - \phi_s}{t_{ox}} = \sqrt{2\varepsilon_{si} k_b T n_i} e^{\frac{q\phi_s}{2k_b T}}. \quad (49)$$

Since $\frac{\varepsilon_{ox}}{t_{ox}} = C_{ox}$, so (49) can be re-written as:

$$C_{ox}(V_g - \Delta\chi_{ms} - \phi_s) = \sqrt{2\varepsilon_{si} k_b T n_i} e^{\frac{q\phi_s}{2k_b T}}. \quad (50)$$

Substituting $V_g - \Delta\chi_{ms} - \phi_s = V_{gt}$ in (50) and on solving:

$$\phi_s = \frac{2k_b T}{q} \ln \left[\frac{C_{ox} V_{gt}}{\sqrt{2\varepsilon_{si} k_b T n_i}} \right] \quad (51)$$

Since the threshold condition is given by:

$$V_{th} = \Delta\chi_{ms} + \phi_s \quad (52)$$

Substituting ϕ_s from (51):

$$V_{th} = \Delta\chi_{ms} + \frac{2k_b T}{q} \ln \left[\frac{C_{ox} V_{gt}}{\sqrt{2\varepsilon_{si} k_b T n_i}} \right]. \quad (53)$$

The V_{th} model (53) is a transcendental equation which needs to be solved numerically. The ϕ_s increases with the increase in V_g , and the ϕ_0 asymptotically approach a constant value: $\phi_{0,max} = (k_b T/q) \ln[2\pi^2 \varepsilon_{si} k_b T / q^2 n_i t_{si}]$ with slope = $2C_{ox}$. Volume inversion takes place in the subthreshold region and volume inversion, no band bending occurs.

2) Chen et al. [18]:

Chen et al. [18] defined the V_{th} as the required V_g at which the inversion charge sheet density Q_{inv} at minimum potential position (virtual cathode) reaches a value Q_{th} which is sufficient enough to turn on the device [33]. Fig. 4 shows the threshold condition defined for DG MOSFETs. The effective conductive path is located at $x = t_{si}/4$ from the top and bottom surfaces. The V_{th} model for the long-channel DG MOSFET is:

$$V_{th} = \Delta\chi_{ms} + V_T \ln \left(\frac{Q_{th}}{n_i t_{si}} \right). \quad (54)$$

The value of Q_{th} is determined as $3.2 \times 10^{10} \text{ cm}^{-2}$. Similar expression (54) has been deduced by Hamid et al. [33].

C. Drain-Current Models

The I_{ds} models can be broadly classified into potential based and charge based models. In the potential based models, the I_{ds} is expressed through indirect function of applied V_g and V_{ds} . Whereas, in charge based models, the I_{ds} is expressed in terms of terminal charges, as an implicit function of V_g and V_{ds} .

1) Taur et al. [19]:

The model [19] is a surface potential based model in which I_{ds} is expressed in terms of applied bias. The pre-requisite for the model is electrostatic potential models [15,16]. The drain current expression is:

$$I_{ds} = \mu \frac{W}{L} \frac{4\epsilon_{si}}{t_{si}} \left(\frac{2k_b T}{q} \right)^2 [g_r(\beta_s) - g_r(\beta_d)] \quad (55)$$

where $g_r(\beta) = \left[\beta \tan \beta - \frac{\beta^2}{2} + 2r\beta^2 \tan^2 \beta \right]$ with β_s and β_d are the values of β at the source and drain ends respectively. Three different equations have been used for subthreshold, linear, and saturation regions by approximating the values of β . The I_{ds} model is based on Pau-Sah's double integral, which is based on GCA [50]. The GCA is valid for most regions of MOSFET operation except beyond the pinch-off point. Charge-sheet model [57] is then introduced to obtain the implicit equations for I_{ds} model. The detailed derivation is as follows.

For the long channel devices, the total electron current density is the sum of the drift and diffusion current density [51,58]:

$$J_n(x, y) = qn(x, y)\mu_n E_x + qD_n \frac{dn(x, y)}{dx}, \quad (56)$$

where $E_x = -d\phi(x)/dx$ is the vertical electric field in the silicon body and $D_n = \mu_n V_T$ is the electron diffusion coefficient [51]. Substituting E_x and D_n in (56):

$$J_n(x, y) = -qn(x, y)\mu_n \left[\frac{d\phi(x)}{dx} - \frac{k_b T}{qn(x, y)} \frac{dn(x, y)}{dx} \right], \quad (57)$$

where $n(x, y) = n_i e^{\frac{q(\phi(x) - \phi_F)}{k_b T}}$ is the electron density. On rearranging the terms of $n(x, y)$:

$$\frac{n(x, y)}{n_i} = e^{\frac{q(\phi(x) - \phi_F)}{k_b T}}, \text{ which on solving will yield:}$$

$$\phi(x) - \frac{k_b T}{q} \ln \left[\frac{n(x, y)}{n_i} \right] = \phi_F. \quad (58)$$

Differentiating (58) with respect to x

$$\frac{d\phi(x)}{dx} - \frac{k_b T}{qn(x, y)} \frac{dn(x, y)}{dx} = \frac{d\phi_F}{dx}. \quad (59)$$

Substituting (59) in (57):

$$J_n(x, y) = -q\mu_n n(x, y) \frac{d\phi_F}{dy}. \quad (60)$$

The I_{ds} is expressed in terms of $J_n(x, y)$ [51] as:

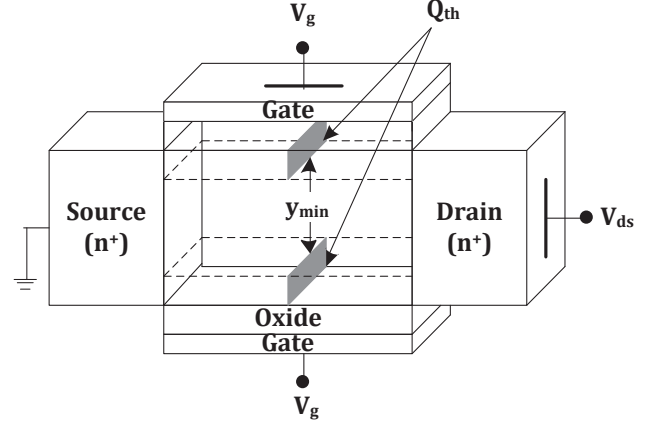


Fig. 4. Schematic showing the inversion charge sheet density at threshold condition. (Dashed lines represent the effective conductive path).

$$I_{ds}(y) = 2W \int_0^{\frac{t_{si}}{2}} -q\mu_n n(x, y) \frac{d\phi_F}{dy} dx. \quad (61)$$

Equation (61) can be written as:

$$I_{ds}(y) = 2W\mu_n (-Q_{inv}(y)) \frac{d\phi_F}{dy}, \quad (62)$$

where $-Q_{inv}(y) = \int_0^{\frac{t_{si}}{2}} qn(x, y) dx$ is the inversion charge sheet density. Integrating the both sides of (62):

$$\int_0^L I_{ds}(y) dy = \mu_n 2W \int_0^{V_{ds}} (-Q_{inv}(y)) d\phi_F, \quad (63)$$

$$I_{ds} = \mu_n \left(\frac{2W}{L} \right) \int_0^{V_{ds}} (-Q_{inv}(y)) d\phi_F.$$

Rearranging the terms of (1) will yield:

$$e^{\frac{\phi(x) - \phi_F}{V_T}} = \left(\frac{2\beta}{t_{si}} \right)^2 \left(\frac{2\epsilon_{si} k_b T}{q^2 n_i} \right) \sec^2 \left(\frac{2\beta}{t_{si}} x \right). \quad (64)$$

On substituting $n(x, y) = n_i e^{\frac{q(\phi(x) - \phi_F)}{k_b T}}$ in the expression $-Q_{inv}(y) = \int_0^{\frac{t_{si}}{2}} qn(x, y) dx$ will yield:

$$-Q_{inv}(y) = q \int_0^{\frac{t_{si}}{2}} n_i e^{\frac{\phi(x) - \phi_F}{V_T}} dx. \quad (65)$$

Substituting (64) in (65):

$$-Q_{inv}(y) = q \int_0^{\frac{t_{si}}{2}} n_i \left(\frac{2\beta}{t_{si}} \right)^2 \left(\frac{2\epsilon_{si} k_b T}{q^2 n_i} \right) \sec^2 \left(\frac{2\beta}{t_{si}} x \right) dx. \quad (66)$$

On solving (66):

$$\begin{aligned} -Q_{inv}(y) &= qn_i \left(\frac{2\beta}{t_{si}} \right)^2 \left(\frac{2\epsilon_{si} k_b T}{q^2 n_i} \right) \left(\frac{t_{si}}{2\beta} \right) \tan \left(\frac{2\beta}{t_{si}} x \right) \Big|_{x=0}^{\frac{t_{si}}{2}} \\ &= qn_i \left(\frac{2\beta}{t_{si}} \right) \left(\frac{2\epsilon_{si} k_b T}{q^2 n_i} \right) \tan(\beta) \\ &= \frac{4\epsilon_{si} k_b T}{qt_{si}} \beta \tan \beta. \end{aligned} \quad (67)$$

$$I_{ds} = \mu_n \left(\frac{2W}{L} \right) \int_0^{V_{ds}} \frac{4\epsilon_{si} k_b T}{qt_{si}} \beta \tan \beta \left[-2V_T \left\{ \frac{1}{\beta} + (2r+1) \tan \beta + 2r\beta \sec^2 \beta \right\} \right] d\beta. \quad (70)$$

Referring to the expression (27):

$$\frac{V_g - \Delta\chi_{ms} - \phi_F}{2V_T} - \ln \left[\frac{2}{t_{si}} \sqrt{\frac{2\varepsilon_{si}k_bT}{q^2n_i}} \right] = \ln \beta - \ln \cos \beta + 2r\beta \tan \beta. \quad (68)$$

Differentiating (68) with respect to β :

$$d\phi_F = -2V_T \left[\frac{1}{\beta} + (2r+1) \tan \beta + 2r\beta \sec^2 \beta \right]. \quad (69)$$

Substituting (67) and (69) in (63) will yield (shown at the bottom of the previous page):

$$\begin{aligned} & \text{Changing the integral limit of (70) from } \int_0^{V_{ds}} d\beta \text{ to } \int_{\beta_s}^{\beta_d} d\beta: \\ I_{ds} &= -\mu_n \left(\frac{2W}{L} \right) \left(\frac{2\varepsilon_{si}}{t_{si}} \right) \left(\frac{2k_bT}{q} \right)^2 \\ & \int_{\beta_s}^{\beta_d} [\tan \beta + (2r+1) \beta \tan^2 \beta + 2r\beta^2 \tan \beta \sec^2 \beta] d\beta \\ &= \mu_n \left(\frac{2W}{L} \right) \left(\frac{2\varepsilon_{si}}{t_{si}} \right) \left(\frac{2k_bT}{q} \right)^2 \left[\int_{\beta_d}^{\beta_s} \tan \beta d\beta + \right. \\ & \quad (2r+1) \int_{\beta_d}^{\beta_s} \beta \tan^2 \beta d\beta + \\ & \quad \left. 2r \int_{\beta_d}^{\beta_s} \beta^2 \tan \beta \sec^2 \beta d\beta \right]. \quad (71) \end{aligned}$$

There are three integrals to be solved in (71) which are: $\int \tan \beta d\beta$, $\int \beta \tan^2 \beta d\beta$, and $\int \beta^2 \tan \beta \sec^2 \beta d\beta$. Solution of the integrals are expressed as:

$$\int \tan \beta d\beta = \ln \sec \beta. \quad (72)$$

$$\begin{aligned} \int \beta \tan^2 \beta d\beta &= \int \beta (\sec^2 \beta - 1) d\beta, \\ &= \int \beta \sec^2 \beta d\beta - \int \beta d\beta \\ &= \beta \tan \beta - \ln \sec \beta - \frac{\beta^2}{2}. \quad (73) \end{aligned}$$

$$\begin{aligned} \int \beta^2 \tan \beta \sec^2 \beta d\beta &= \beta^2 \tan \beta \int \sec^2 \beta d\beta - \\ & \quad \int \left\{ \frac{d}{d\beta} \beta^2 \tan \beta \int \sec^2 \beta d\beta \right\} d\beta \\ &= \frac{1}{2} \beta^2 \tan^2 \beta - \beta \tan \beta + \ln \sec \beta + \frac{\beta^2}{2}. \quad (74) \end{aligned}$$

Substituting (72–74) in (71) will yield:

$$I_{ds} = \mu_n \left(\frac{2W}{L} \right) \left(\frac{2\varepsilon_{si}}{t_{si}} \right) \left(\frac{2k_bT}{q} \right)^2 \left[\beta \tan \beta - \frac{\beta^2}{2} + r\beta^2 \tan^2 \beta \right] \Big|_{\beta=\beta_d}^{\beta_s}. \quad (75)$$

Equating the terms: $\ln \beta - \ln \cos \beta + 2r\beta \tan \beta = f_r(\beta)$ [from (68)] and $\beta \tan \beta - \frac{\beta^2}{2} + r\beta^2 \tan^2 \beta = g_r(\beta)$ [from (55) and (75)]. At source end $\beta = \beta_s$ and $\phi_F = 0$ V. So,

$$\begin{aligned} f_r(\beta_s) &= \frac{V_g - \Delta\chi_{ms}}{2V_T} - \ln \left[\frac{2}{t_{si}} \sqrt{\frac{2\varepsilon_{si}k_bT}{q^2n_i}} \right] \\ &= \frac{V_g - \left(\Delta\chi_{ms} + 2V_T \ln \left[\frac{2}{t_{si}} \sqrt{\frac{2\varepsilon_{si}k_bT}{q^2n_i}} \right] \right)}{2V_T} \\ &= \frac{V_g - V_0}{2V_T}. \quad (76) \end{aligned}$$

where $V_0 = \Delta\chi_{ms} + 2V_T \ln \left[\frac{2}{t_{si}} \sqrt{\frac{2\varepsilon_{si}k_bT}{q^2n_i}} \right]$. At drain end, $\beta = \beta_d$ and $\phi_F = V_{ds}$. So,

$$f_r(\beta_d) = \frac{V_g - V_0 - V_{ds}}{2V_T}. \quad (77)$$

In the linear region of operation, $f_r(\beta_s) = f_r(\beta_d) \gg 1$ which implies $\beta_s, \beta_d > \frac{\pi}{2}$. So, the term $f_r(\beta)$ in (76) and $g_r(\beta)$ in (77) are reduced to $2r\beta \tan \beta$ and $r\beta^2 \tan^2 \beta$ respectively. Therefore,

$$f_r(\beta_s) \equiv \beta_s \tan \beta_s = \left(\frac{V_g - V_0}{2V_T} \right) \frac{1}{2r}. \quad (78)$$

$$\text{Similarly, } f_r(\beta_d) \equiv \beta_d \tan \beta_d = \left(\frac{V_g - V_0 - V_{ds}}{2V_T} \right) \frac{1}{2r}, \quad (79)$$

and the expression (75) reduces to:

$$I_{ds,LIN} = \mu_n \frac{2W}{L} \frac{2\varepsilon_{si}}{t_{si}} (2V_T)^2 [r\beta^2 \tan^2 \beta]_{\beta_d}^{\beta_s}. \quad (80)$$

On substituting (78) and (79) in (80) :

$$\begin{aligned} I_{ds,LIN} &= \mu_n \frac{2W}{L} \frac{2\varepsilon_{si}}{t_{si}} (2V_T)^2 \frac{1}{4r} \left[\left(\frac{V_g - V_0}{2V_T} \right)^2 - \left(\frac{V_g - V_0 - V_{ds}}{2V_T} \right)^2 \right] \\ &= \mu_n \frac{W}{L} C_{ox} \left[(V_g - V_0)^2 - (V_g - V_0 - V_{ds})^2 - V_{ds}^2 + 2(V_g - V_0)V_{ds} \right] \\ &= 2\mu_n \frac{W}{L} C_{ox} \left[(V_g - V_{th}) - \frac{V_{ds}}{2} \right] V_{ds}, \quad (81) \end{aligned}$$

where $V_{th} = V_0 + \delta$, δ is the second-order effects. The $I_{ds,LIN}$ (81) is the drain current expression for the linear region. The δ is derived as follows.

Considering $\phi_F = 0$ in (25), the ϕ_s at the source region is expressed as: $\phi_s = -\frac{2k_bT}{q} \ln \left[\frac{t_{si}}{2\beta} \sqrt{\frac{q^2n_i}{2\varepsilon_{si}k_bT}} \cos(\beta) \right]$. Since the threshold condition is given by: $V_{th} = \Delta\chi_{ms} + \phi_s$ [15], the expression of the V_{th} in (81) is written as:

$$\begin{aligned} V_{th} &= \Delta\chi_{ms} - \frac{2k_bT}{q} \ln \left[\frac{t_{si}}{2} \sqrt{\frac{q^2n_i}{2\varepsilon_{si}k_bT}} \right] - \frac{2k_bT}{q} \ln \frac{\cos \beta}{\beta} \\ &= V_0 + \frac{2k_bT}{q} \ln \frac{\beta}{\cos \beta} \\ &= V_0 + \frac{2k_bT}{q} \ln \frac{\beta \sin \beta}{\cos \beta \sin \beta} \\ &= V_0 + \frac{2k_bT}{q} \ln \beta \tan \beta - \frac{2k_bT}{q} \ln \sin \beta. \quad (82) \end{aligned}$$

In the strong inversion condition, the $\beta \rightarrow \frac{\pi}{2}$ which implies the term “ $\ln \sin \beta$ ” in (82) is ≈ 0 . So,

$$V_{th} = V_0 + \frac{2k_bT}{q} \ln \beta \tan \beta = V_0 + \delta, \quad (83)$$

with $\delta = (2k_bT/q) \ln \beta \tan \beta$. Substituting (78) in (83) will yield:

$$\delta = \frac{2k_bT}{q} \ln \left[\left(\frac{V_g - V_0}{2V_T} \right) \frac{1}{2r} \right]. \quad (84)$$

Equation (84) is the second-order effect $\approx 0.05V$.

In the saturation region of operation, $\beta_s \approx \pi/2$ and $\beta_d \ll 1$. So, the terms $f_r(\beta_s)$ and $f_r(\beta_d)$ are reduced to $2r\beta_s \tan \beta_s$ and

In β_d respectively. Therefore,

$$f_r(\beta_s) \equiv r\beta_s \tan \beta_s = \left(\frac{V_g - V_o}{4V_T}\right) \quad (85)$$

$$\text{and } f_r(\beta_d) \equiv \beta_d = e^{\left(\frac{V_g - V_o - V_{ds}}{2V_T}\right)}. \quad (86)$$

The expression (75) reduces to :

$$I_{ds,SAT} = \mu_n \frac{2W}{L} \frac{2\epsilon_{si}}{t_{si}} (2V_T)^2 \left[r\beta_s^2 \tan^2 \beta_s - \frac{\beta_d^2}{2} \right]. \quad (87)$$

Substituting (85) and (86) in (87) will yield:

$$\begin{aligned} I_{ds,SAT} &= \mu_n \frac{2W}{L} \frac{2\epsilon_{si}}{t_{si}} (2V_T)^2 \left[r \left(\frac{V_g - V_o}{4V_T}\right)^2 - \frac{1}{2} e^{\left(\frac{V_g - V_o - V_{ds}}{V_T}\right)} \right] \\ &= \mu_n \frac{W}{L} C_{ox} \left[(V_g - V_o)^2 - \frac{8rk_b^2 T^2}{q^2} e^{\left(\frac{V_g - V_o - V_{ds}}{V_T}\right)} \right]. \end{aligned} \quad (88)$$

Equation (88) is the drain current expression for the saturation region ($I_{ds,SAT}$).

In subthreshold region of operation, $\beta_s, \beta_d \ll 1$. So the terms $f_r(\beta)$ and $g_r(\beta)$ are reduced to $\ln \beta$ and $(\beta/2)$ respectively. On solving (76) for $f_r(\beta) = \ln \beta$ will yield:

$$\ln \beta_s = \frac{V_g - V_o}{2V_T} \equiv \frac{V_g - \Delta\chi_{ms}}{2V_T} - \ln \left[\frac{2}{t_{si}} \sqrt{\frac{2\epsilon_{si}k_b T}{q^2 n_i}} \right],$$

which implies:

$$\beta_s = \frac{2}{t_{si}} \sqrt{\frac{2\epsilon_{si}k_b T}{q^2 n_i}} e^{\frac{V_g - \Delta\chi_{ms}}{2V_T}}. \quad (89)$$

Similarly,

$$\beta_d = \frac{2}{t_{si}} \sqrt{\frac{2\epsilon_{si}k_b T}{q^2 n_i}} e^{\frac{V_g - \Delta\chi_{ms} - V_{ds}}{2V_T}} \quad (90)$$

Since $g_r(\beta) = \frac{\beta}{2}$, the (75) reduces to:

$$I_{ds,SUB} = \mu_n \frac{2W}{L} \frac{2\epsilon_{si}}{t_{si}} (2V_T)^2 \left[\frac{\beta_s^2}{2} - \frac{\beta_d^2}{2} \right] \quad (91)$$

On substituting (89) and (90) in (91) will finally yield the $I_{ds,SUB}$ model for the subthreshold region.

$$I_{ds,SUB} = \mu_n \frac{W}{L} k_b T n_i t_{si} e^{\frac{V_g - \Delta\chi_{ms}}{V_T}} \left(1 - e^{\frac{-V_{ds}}{V_T}} \right) \quad (92)$$

Combining the $I_{ds,LIN}$ (81), $I_{ds,SAT}$ (88), and $I_{ds,SUB}$ (92) for the different regions namely linear, saturation, and subthreshold, respectively, the complete I_{ds} model is written as:

$$I_{ds} = \begin{cases} \mu \frac{W}{L} V_T q n_i t_{si} e^{\frac{V_{gs} - \Delta\chi_{ms}}{V_T}} \left(1 - e^{\frac{-V_{ds}}{V_T}} \right) \\ 2\mu C_{ox} \frac{W}{L} \left(V_{gs} - V_{th} - \frac{V_{ds}}{2} \right) V_{ds} \\ \mu C_{ox} \frac{W}{L} \left[(V_{gs} - V_{th}) - 8rV_T^2 e^{\frac{V_{gs} - V_o - V_{ds}}{V_T}} \right] \end{cases} \quad (93)$$

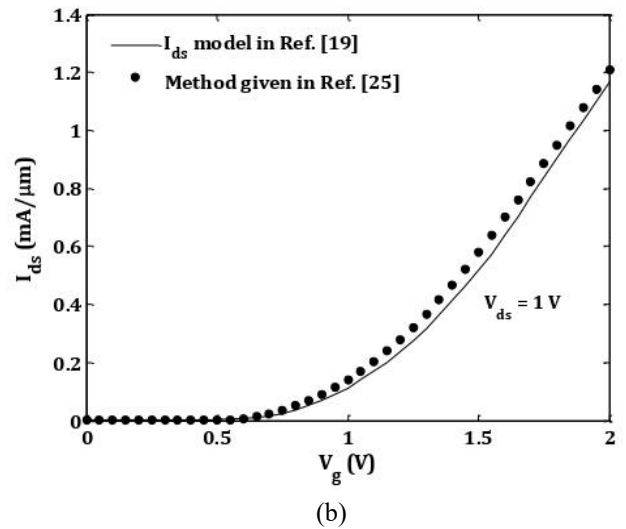
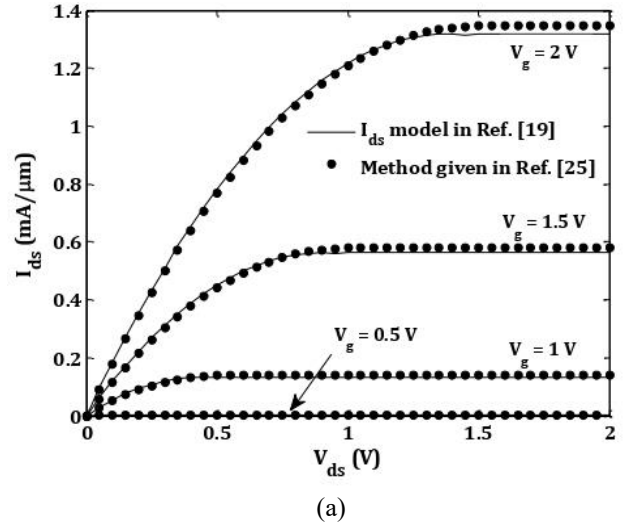


Fig. 5. Characteristics of a long-channel DG MOSFET with $L = 1 \mu\text{m}$, $W = 1 \mu\text{m}$, $t_{si} = 5 \text{ nm}$, and $t_{ox} = 1.5 \text{ nm}$ obtained from model (93) in comparison with the results obtained through using the method given by Yu *et al.* [25] (a) output characteristics, (b) transfer characteristics.

Equation (93) is the long channel core I_{ds} model for DG MOSFETs which has been subsequently augmented with various physical effects like SCE, quantum mechanical effect, and low and high field transport in order to develop I_{ds} models [22, 23] for short-channel DG MOSFETs. Fig. 5 shows the I_{ds} characteristics obtained from (93) for an undoped DG MOSFET with a mid-gap metal gate, in comparison with the characteristics obtained through solving the β from (27) by the method given by Yu *et al.* [25]. A constant mobility $\mu_n = 300 \text{ cm}^2/(\text{Vs})$ [19,25,26] has been considered in numerical simulation. The I_{ds} models in [19, 22–27] are based on assumptions of constant electron mobility in order to validate the results with the simulated data. Constant mobility in the I_{ds} model is a strong assumption [59] since the mobility gets affected by the vertical and horizontal electric field due to the V_g and V_{ds} respectively. The I_{ds} models [28, 29] considered the Caughey-Thomas mobility model [60] while the models in [30,

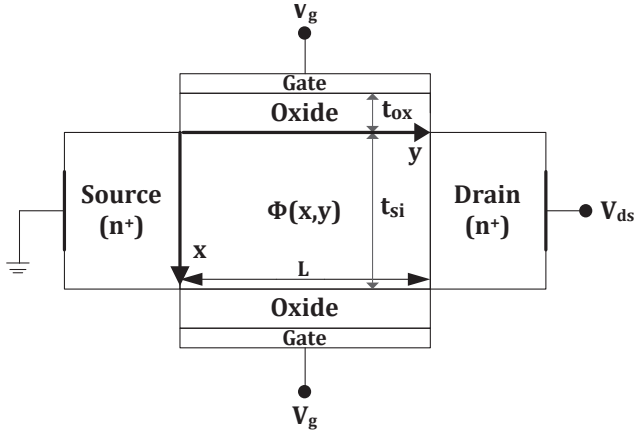


Fig. 6. The cross-sectional view of a short-channel n-type symmetric DG MOSFET along with the geometrical coordinates.

31] took into account the Lombardi CVT mobility model [61] to depict the drain current characteristics.

III. MODELS FOR SHORT CHANNEL DG MOSFETS

A. Electrostatic Potential Models

In the short-channel devices, due to SCEs the electric fields from the source and drain encroach horizontally into the channel and thus introduce a second dimension (y) [Fig. 6] to the channel electrostatics $\phi(x,y)$ [11]. The modeling for nanoscale (short-channel) DG MOSFETs solves 2-D Poisson's equation in order to derive the analytical $\phi(x,y)$ model. The approach adopted in [33–35], derived the $\phi(x,y)$ using superposition method where the 2-D Poisson's equation split into 1-D Poisson and 2-D Laplace equation. The reported papers [20],[32],[36–38] adopted parabolic potential approximation, where $\phi(x,y)$ is obtained using a parabolic function in terms of x and y . This section describes the $\phi(x,y)$ model given by Tsormpatzoglou *et al.* [20] in order to address the modeling scheme for short-channel ($L = 30$ nm) DG MOSFET.

1) Tsormpatzoglou *et al.* [20]:

Tsormpatzoglou *et al.* [20] presented an analytical expression (94) of the $\phi(x,y)$ along the channel of lightly-doped symmetrical DG MOSFET in weak inversion:

$$\phi(x,y) = \frac{1}{e^{\frac{2L}{\lambda_x} - 1}} \left[(V_{bi} + V_{ds} - A_x) \left(e^{\frac{L+y}{\lambda_x}} - e^{\frac{L-y}{\lambda_x}} \right) + (V_{bi} - A_x) \left(e^{\frac{2L-y}{\lambda_x}} - e^{\frac{y}{\lambda_x}} \right) + A_x \left(e^{\frac{2L}{\lambda_x}} - 1 \right) \right], \quad (94)$$

with $A_x = V_g - \Delta\chi_{ms} - qN_{si} \frac{\epsilon_{si} t_{ox} t_{si} + \epsilon_{ox} (t_{si} - x)x}{2\epsilon_{ox}\epsilon_{si}}$. In case of a lightly-doped body, $\Delta\chi_{ms} = -V_T \ln(N_{si}/n_i)$ for mid-gap metal gates [Fig. 3], $V_{bi} = V_T \ln(N_{si}N_{sd}/n_i^2)$ is the built-in potential, and N_{sd} is the doping concentration of source and drain. $\lambda_x =$

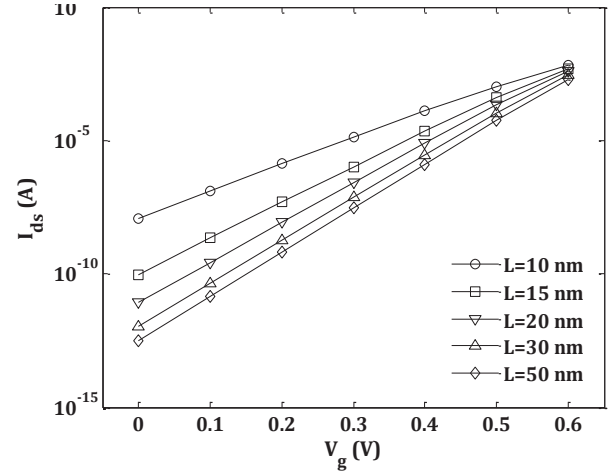


Fig. 7. Transfer characteristics (in semi-logarithmic scale) in the subthreshold region of short-channel DG MOSFET obtained from solving (97) through the numerical method.

$\sqrt{\frac{\epsilon_{si} t_{ox} t_{si}}{2\epsilon_{ox}} \left(1 + \frac{\epsilon_{ox} x}{\epsilon_{si} t_{ox}} - \frac{\epsilon_{ox} x^2}{\epsilon_{si} t_{ox} t_{si}} \right)}$ is the natural channel length proposed by Yan *et al.* [9] which is described more accurately as a function channel depth in short-channel devices. The 2-D extra potential $\Delta\phi(x,y)$ induced in the channel due to SCEs is described by:

$$\Delta\phi(x,y) = \frac{1}{e^{\frac{2L}{\lambda_x} - 1}} \left[(V_{bi} + V_{ds} - A_x) \left(e^{\frac{L+y}{\lambda_x}} - e^{\frac{L-y}{\lambda_x}} \right) + (V_{bi} - A_x) \left(e^{\frac{2L-y}{\lambda_x}} - e^{\frac{y}{\lambda_x}} \right) \right]. \quad (95)$$

Based on the 2-D extra potential induced in the channel due to SCEs, a semi-analytical expression for the subthreshold drain current is derived. In the subthreshold condition, the diffusion current dominates due to weak inversion [62]. For weak inversion, the drain current in the subthreshold condition of a long channel device can be expressed as:

$$I_{ds,long} = \frac{W}{L} V_T \mu_n Q_{is} \left(1 - e^{-\frac{V_{ds}}{V_T}} \right), \quad (96)$$

where $Q_{is} = \frac{qn_i^2}{N_{si}} t_{si} e^{\frac{\phi_s}{V_T}}$ is the inversion charge sheet density at the source end, and $\phi_s = A_{x=0}$ is the surface potential for long channel device. The drain current expression for a short-channel device is obtained by dividing the long channel case by correction factor (CF).

$$I_{ds,short} = \frac{W}{L} V_T \mu_n Q_{is} \frac{1}{CF} \left(1 - e^{-\frac{V_{ds}}{V_T}} \right), \quad (97)$$

where $CF = \frac{1}{L} \int_0^L \frac{1}{t_{si}} \int_0^{t_{si}} e^{-\frac{\Delta\phi(x,y)}{V_T}} dx dy$. Here, the CF has to be calculated numerically and hence the model is not applicable in developing a compact model for DG MOSFETs. However, the same can be used to properly design new DG MOSFETs

because it is rather a semi-analytical model of SCE. Also, equation (97) allows extrapolation of various DG device specifications. The subthreshold drain current characteristics of DG MOSFET shown in Fig. 7 with $W = 1\mu\text{m}$, $t_{si} = 5\text{ nm}$, $t_{ox} = 1\text{ nm}$, and $\mu_n = 500\text{ cm}^2/\text{Vs}$ for different values of L at $V_{ds} = 0.02\text{ V}$ have been implemented using MATLAB. In addition, Simpson's one-third method [54] has been employed to evaluate the CF .

The MATLAB code to obtain the subthreshold drain current characteristics [Fig. 7]

```

W=1000*10^(-9);           % Channel width
tsi=5*10^(-9);           % Body thickness
tox=1*10^(-9);           % Gate oxide thickness
Eo=8.85*10^(-12);        % Permittivity of free space
Eox=3.9*Eo;              % Dielectric permittivity of oxide
Esi=11.68*Eo;            % _____ of silicon
Nsi=10^(21);              % Body doping density
Nsd=5*(10^25);           % S/D doping density
ni=1.45*10^(16);         % Intrinsic charge concentration
L=[10 15 20 30 50]*10^(-9); % Different// channel lengths considered
u=500*10^(-4);          % Mobility of electrons
K=1.38*10^(-23);        % Boltzmann constant
T=300;                  % Room temperature
q=1.6*10^(-19);         % Elementary charge
VT=(K*T)/q;             % Thermal voltage = 26mV
Vbi=VT*log(Nsi*Nsd/(ni^2)); % Built-in potential
Vfb=-VT*log(Nsi/ni);    % Flat band voltage
Vds=0.02;               % Drain to source voltage
Vg=0:0.1:0.6;          % Gate voltage sweep
Cox=Eox/tox;            % Oxide capacitance
%----- Simpson's 1/3rd method begins----- %
h1=((tsi-0)/10);
x=[0 h1 2*h1 3*h1 4*h1 5*h1 6*h1 7*h1 8*h1 9*h1 10*h1];
for l=1:length(L)
h2=(L(l)-0)/10;
y=[0 h2 2*h2 3*h2 4*h2 5*h2 6*h2 7*h2 8*h2 9*h2 10*h2];

for k=1:length(Vgs)
Vg(k)=Vgs(k)-Vfb;
for j=1:length(y)
for i=1:length(x)
xterm(i)=(1+((Eox*x(i))/(Esi*tox))-
((Eox*(x(i)^2))/(Esi*tox*tsi)));
lambda(i)=sqrt(((Esi*tox*tsi)/(2*Eox))*xterm(i))
;
delphi(i)=(1/(exp((2*L(l))/lambda(i))-1))*((Vbi+Vd-Vg(k))*(exp((L(l)+y(j))/lambda(i))-exp((L(l)-y(j))/lambda(i)))+(Vbi-Vg(k))*(exp((2*L(l)-y(j))/lambda(i))-exp(y(j)/lambda(i))));
f(i)=exp(-(delphi(i))/VT);
end

```

```

I1(j)=(h1/3)*((f(1)+f(11))+4*(f(2)+f(4)+f(6)+f(8)+f(10))+2*(f(3)+f(5)+f(7)+f(9)));
End

I2(k)=(h2/3)*((I1(1)+I1(11))+4*(I1(2)+I1(4)+I1(6)+I1(8))+2*(I1(3)+I1(5)+I1(7)+I1(9)));
CF(k)=(1/(tsi*L(1)))*I2(k);
phis(k)=(Vgs(k)-Vfb)-((q*Nsi*tsi)/(2*Cox));

Qis(k)=(q*(ni^2)/Nsi)*tsi*exp((q*phis(k))/(K*T))
;
Id(1,k)=(W/L(1))*(K*T/q)*u*Qis(k)*(1/CF(k))*(1-exp((-q*Vd)/(K*T)));
end
end
plot(Vg, log10(Id(1,:)), Vg, log10(Id(2,:)), Vg, log10(Id(3,:)), Vg, log10(Id(4,:)), Vg, log10(Id(5,:)));
xlabel('V_{g} (V)');
ylabel('I_{ds} (A)')

```

The ϕ model (94) is derived based on the solution of 2-D Poisson's equation under the consideration of fixed charge density only; hence the model is not valid in strong inversion regime. Notable ϕ models [33–35] are derived using the superposition method to validate the same in strong inversion regime. Validity of any ϕ model in the strong inversion regime signifies that the model can depict the variation in electrostatic potential characteristics with respect to the change in V_g . Hamid *et al.* [33] derived the ϕ model considering only the effect of mobile charge density in the 2-D Poisson's equation. The concept of cross-over point [63], which was not put into emphasis in [33], has been discussed later in the ϕ model given Ray and Mahapatra [34]. The ϕ models given by Oh *et al.* [35] and Liang *et al.* [39] did not consider both fixed as well as mobile charge densities, however, Liang *et al.* [39] derived the ϕ model by the scale length method [64]. The ϕ modeling scheme including the fixed charge density in the 2-D Poisson's equation has been further extended by Pandey *et al.* [40] and the same was solved through the Green's function method [65]. Despite differences in mathematical equations, the potential distribution characteristics generated by the ϕ models in [39] and [40] are found to be consistent with each other.

B. Threshold Voltage Models

1) Tsormpatzoglou *et al.* [21]:

A V_{th} model in [21] of an undoped symmetrical DG MOSFET developed based on the $\phi(x, y)$ model (94) given by Tsormpatzoglou *et al.* [20]. This short-channel V_{th} model was derived by considering only the fixed charge density in Poisson's equation subjected to the condition $L/t_{si} > 2$. The channel position at which the potential along the effective conductive path reaches to its minimum value is called virtual cathode (y_{min}), which plays an important role in deriving the threshold voltage expression. The explicit expression for V_{th} is given as:

$$V_{th} = \Delta\chi_{ms} + AV_T \ln\left(\frac{Q_{th}}{n_i t_{si}}\right) \quad (98)$$

$$-B \left[V_{bi} - V_T \ln \left(\frac{Q_{th}}{n_i t_{si}} \right) \right]^{\frac{1}{2}} \left[V_{bi} + V_{ds} - V_T \ln \left(\frac{Q_{th}}{n_i t_{si}} \right) \right]^{\frac{1}{2}} - C (2V_{bi} + V_{ds}),$$

$$\text{where } A = \frac{\left(e^{\frac{4L}{\lambda} - 2e^{\frac{2L}{\lambda} + 1}} \right)}{\left(e^{\frac{2L}{\lambda} - 1} \right)^4}, \quad B = \frac{\frac{L}{2e^{2\lambda}} \left(e^{\frac{L}{\lambda} + 1} \right)}{\left(e^{\frac{2L}{\lambda} - 1} \right)^2}, \quad C = \frac{2 \left(e^{\frac{3L}{\lambda} - 2e^{\frac{2L}{\lambda} + 1}} \right)}{\left(e^{\frac{2L}{\lambda} - 1} \right)^4}.$$

λ is the natural channel length along the effective conductive path $= \sqrt{\frac{\epsilon_{si} t_{ox} t_{si}}{2\epsilon_{ox}} \left(1 + \frac{\epsilon_{ox} t_{si}}{4\epsilon_{si} t_{ox}} - \frac{\epsilon_{ox} t_{si}}{16\epsilon_{si} t_{ox}} \right)}$. For long channel device, $A=1$, and the parameter B and C tend to zero and thus, the V_{th} expression reduces to that of a long-channel DG MOSFET: $V_{th} = \Delta\chi_{ms} + V_T \ln \left(\frac{Q_{th}}{n_i t_{si}} \right)$ as given by Chen *et al.* [18]. The Q_{th} for long channel DG MOSFET has been determined to be about $= 3.2 \times 10^{10} \text{cm}^{-2}$. Whereas, for a short-channel device, the Q_{th} is dependent upon the L , t_{ox} , t_{si} , and V_{ds} by the relationship:

$$Q_{th} = 10^{11} \left[1 - (5 + V_{ds}) \frac{\lambda}{2L} \right]^2 \text{cm}^{-2}. \quad (99)$$

C. Drain-Current Models

1) Tsormpatzoglou *et al.* [22]:

In this model, instead of the numerical approach, an analytical approach is adopted. Various effects like SCEs, series resistance, and CLM are included. Two different equations for subthreshold $I_{ds,SUB}$ and strong inversion $I_{ds,SI}$ have been combined through interpolation method. The detailed derivation of $I_{ds,SI}$ is as follows.

The ϕ model in [16] has been utilized to model the $I_{ds,SI}$, and the model derivation starts from the expression (27), which will imply:

$$\ln \frac{\beta}{\cos \beta} + 2r\beta \tan \beta = \frac{V_g - \Delta\chi_{ms} - \phi_F}{2V_T} - \ln \left[\frac{2}{t_{si}} \sqrt{\frac{2\epsilon_{si} k_b T}{q^2 n_i}} \right], \quad (100)$$

$$\ln \frac{\beta \sin \beta}{\cos \beta \sin \beta} + 2r\beta \tan \beta = \frac{V_g - \Delta\chi_{ms} - \phi_F}{2V_T} - \ln \left[\frac{2}{t_{si}} \sqrt{\frac{2\epsilon_{si} k_b T}{q^2 n_i}} \right], \quad (101)$$

$$\ln \beta \tan \beta - \ln \sin \beta + 2r\beta \tan \beta = \frac{V_g - \Delta\chi_{ms} - \phi_F}{2V_T} - \ln \left[\frac{2}{t_{si}} \sqrt{\frac{2\epsilon_{si} k_b T}{q^2 n_i}} \right], \quad (102)$$

Replacing the term “ $\beta \tan \beta$ ” in the $Q_{inv}(y)$ expression (67) by q_i (normalized charge density) and substituting in (63) will yield the $I_{ds,SI}$ expression as:

$$I_{ds,SI} = \mu_n \left(\frac{2W}{L} \right) \int_0^{V_{ds}} \frac{4\epsilon_{si} k_b T}{q t_{si}} q_i d\phi_F. \quad (103)$$

In strong inversion, $\beta \rightarrow (\pi/2)$, implies that (102) reduces to:

$$\ln \beta \tan \beta + 2r\beta \tan \beta = \frac{V_g - \Delta\chi_{ms} - \phi_F}{2V_T} - \ln \left[\frac{2}{t_{si}} \sqrt{\frac{2\epsilon_{si} k_b T}{q^2 n_i}} \right]. \quad (104)$$

Substituting q_i in (104):

$$\ln q_i + 2r q_i = \frac{V_g - \Delta\chi_{ms} - \phi_F}{2V_T} - \ln \left[\frac{2}{t_{si}} \sqrt{\frac{2\epsilon_{si} k_b T}{q^2 n_i}} \right]. \quad (105)$$

Differentiating (105) with respect to q_i will yield: $d\phi_F = -2V_T [2r + (1/q_i)] dq_i$. On substituting the $d\phi_F$ in (103):

$$\begin{aligned} I_{ds,SI} &= -\mu_n \left(\frac{2W}{L} \right) \int_{q_{is}}^{q_{id}} \frac{4\epsilon_{si} k_b T}{q t_{si}} q_i 2V_T \left(2r + \frac{1}{q_i} \right) dq_i \\ &= \mu_n \left(\frac{2W}{L} \right) \left(\frac{2\epsilon_{si}}{t_{si}} \right) \left(\frac{2k_b T}{q} \right)^2 \left[2r \frac{q_i^2}{2} + q_i \right]_{q_{is}}^{q_{id}} \\ &= \mu_n \left(\frac{2W}{L} \right) \left(\frac{2\epsilon_{si}}{t_{si}} \right) \left(\frac{2k_b T}{q} \right)^2 \left[(q_{is} - q_{id}) + \frac{\epsilon_{si} t_{ox}}{\epsilon_{ox} t_{si}} (q_{is}^2 - q_{id}^2) \right], \end{aligned} \quad (106)$$

where q_{is} , q_{id} are the values of q_i at source ($\phi_F = 0$) and drain ($\phi_F = V_{ds}$) ends respectively. The expression for q_i can be derived from (105) as:

$$\ln \left[\frac{2q_i}{t_{si}} \sqrt{\frac{2\epsilon_{si} k_b T}{q^2 n_i}} \right] = \frac{q(V_g - \Delta\chi_{ms} - \phi_F)}{2k_b T} - \frac{2\epsilon_{si} t_{ox}}{\epsilon_{ox} t_{si}} q_i. \quad (107)$$

On rearranging the terms of (107):

$$q_i e^{\frac{2\epsilon_{si} t_{ox}}{\epsilon_{ox} t_{si}} q_i} = \frac{t_{si}}{2} \sqrt{\frac{q^2 n_i}{2\epsilon_{si} k_b T}} e^{\frac{q(V_g - \Delta\chi_{ms} - \phi_F)}{2k_b T}}. \quad (108)$$

Multiplying on both sides of (108) by $(2\epsilon_{si} t_{ox} / \epsilon_{ox} t_{si})$:

$$\frac{2\epsilon_{si} t_{ox}}{\epsilon_{ox} t_{si}} q_i e^{\frac{2\epsilon_{si} t_{ox}}{\epsilon_{ox} t_{si}} q_i} = \frac{q t_{ox}}{\epsilon_{ox}} \sqrt{\frac{n_i \epsilon_{si}}{2k_b T}} e^{\frac{q(V_g - \Delta\chi_{ms} - \phi_F)}{2k_b T}} \quad (109)$$

Since, $W e^W = x \Rightarrow W = \text{Lambert}W(x)$, so (109) can be transformed using the Lambert W function:

$$\frac{2\epsilon_{si} t_{ox}}{\epsilon_{ox} t_{si}} q_i = \text{Lambert}W \left[\frac{q t_{ox}}{\epsilon_{ox}} \sqrt{\frac{n_i \epsilon_{si}}{2k_b T}} e^{\frac{q(V_g - \Delta\chi_{ms} - \phi_F)}{2k_b T}} \right],$$

which will imply:

$$q_i = \frac{\epsilon_{ox} t_{si}}{2\epsilon_{si} t_{ox}} \text{Lambert}W \left[\frac{q t_{ox}}{\epsilon_{ox}} \sqrt{\frac{n_i \epsilon_{si}}{2k_b T}} e^{\frac{q(V_g - \Delta\chi_{ms} - \phi_F)}{2k_b T}} \right]. \quad (110)$$

The Lambert $W(x)$ function in current expression was first introduced by Ortiz-Conde *et al.* [66]. When the channel is lightly doped, i.e. $n = (n_i^2 / N_{si})$ and to incorporate threshold voltage roll-off effect, ΔV_{th} is introduced in (110):

$$q_i = \frac{\epsilon_{ox} t_{si}}{2\epsilon_{si} t_{ox}} \text{Lambert}W \left[\frac{q t_{ox}}{\epsilon_{ox}} \sqrt{\frac{n_i^2 \epsilon_{si}}{2k_b T N_{si}}} e^{\frac{q(V_g - \Delta\chi_{ms} + \Delta V_{th} - \phi_F)}{2k_b T}} \right]. \quad (111)$$

A compact I_{ds} model is obtained by combining the $I_{ds,SI}$ and $I_{ds,SUB}$ through interpolation function.

$$I_{ds} = \frac{I_{ds,SI} \times I_{ds,SUB}}{\left(I_{ds,SI}^m + I_{ds,SUB}^m \right)^{\frac{1}{m}}} \quad (112)$$

where $I_{ds,SUB} = \mu_n \left(\frac{2W}{L}\right) \left(\frac{\varepsilon_{ox}}{t_{ox}}\right) \left(\frac{k_b T}{q}\right)^2 e^{1.8} e^{\frac{V_g - V_{th}}{\eta V_T}} \left[1 + e^{\frac{-V_{ds}}{V_T}}\right]$

and $m = 1.9 - \sqrt{1.2V_{ds}}$ is a parameter that prevents the discontinuity in current characteristics at the transition from subthreshold to above-threshold region.

2) *Papathanasiou et al. [23]*:

This model is an improvement over the I_{ds} model given by Tsormpatzoglou *et al.* [22]. Papathanasiou *et al.* [23] provided only one equation for I_{ds} which is valid in all region of operation whereas in [22], two equations were combined through interpolation function. The detailed derivation of I_{ds} model is as follows.

In the subthreshold regime ($V_g < V_{th}$), q_i^2 term in (106) can be approximated as zero, i.e. ($q_i^2 \approx 0$) which implies: $q_i \rightarrow \text{Exp}[q(V_g - \Delta\chi_{ms} + \Delta V_{th} - \phi_F)/2k_b T]$. So, the expression (106) reduces to:

$$\begin{aligned} I_{ds,SI} &= \mu_n \left(\frac{2W}{L}\right) \left(\frac{2\varepsilon_{si}}{t_{si}}\right) \left(\frac{2k_b T}{q}\right)^2 \left[\frac{q_{is}}{2r} - \frac{q_{id}}{2r}\right] \\ &= \mu_n \left(\frac{2W}{L}\right) \left(\frac{4\varepsilon_{ox}}{t_{ox}}\right) \left(\frac{2k_b T}{q}\right)^2 [q_{is} - q_{id}]. \end{aligned} \quad (113)$$

The $I_{ds,SUB}$ can be approximated as [22]:

$$I_{ds,SUB} = \mu_n \left(\frac{2W}{L}\right) \left(\frac{\varepsilon_{ox}}{t_{ox}}\right) \left(\frac{k_b T}{q}\right)^2 e^{0.8} [q_{is,SUB} - q_{id,SUB}], \quad (114)$$

where $q_{i,SUB} = \text{Exp}[q(V_g - V_{th} + \Delta V_{th} - \phi_F)/\eta k_b T]$ and $\eta = (SS/V_T) \ln 10$. On dividing the (114) by (113) will yield:

$$\begin{aligned} \frac{I_{ds,SUB}}{I_{ds,SI}} &= \frac{e^{0.8} e^{\frac{q(V_g - V_{th} - \phi_F)}{\eta k_b T}}}{4 \frac{q(V_g - \Delta\chi_{ms} - \phi_F)}{2k_b T}} \\ &= \frac{e^{0.8} e^{\frac{q(V_g - V_{th} - \phi_F)}{\eta k_b T}}}{4 \frac{q(V_g - V_{th} - \phi_F + V_{th} - \Delta\chi_{ms})}{2k_b T}} \\ &= \frac{e^{0.8} e^{\frac{q(V_g - V_{th} - \phi_F)}{\eta k_b T}}}{4 \frac{q(V_{th} - \Delta\chi_{ms})}{2k_b T}} \\ &= \frac{e^{\frac{q(V_g - V_{th} - \phi_F)}{2\eta_{eff} k_b T}}}{\frac{4}{e^{0.8} e^{\frac{q(V_{th} - \Delta\chi_{ms})}{2k_b T}}}}, \end{aligned} \quad (115)$$

where $V_{ge} = V_g + \Delta V_{th}$ and $\eta_{eff} = \frac{2-\eta}{\eta}$.

In the paper [23], (115) is expressed as:

$$\frac{I_{ds,SUB}}{I_{ds,SI}} = \frac{e^{\frac{q(V_{ge} - V_{th} - \phi_F)}{2\eta_{eff} k_b T}}}{\frac{4}{e^{0.8} e^{\frac{q(V_{th} + \Delta\chi_{ms})}{1V}}}} \quad (116)$$

In this model, only one equation has to be used for both the subthreshold and strong inversion regime. So, it is decided to investigate the possibility of altering the z parameter of Lambert $W(z)$ in q_i , to accommodate for the change in slope of the exponent, at the point where the DG MOSFET is entering the subthreshold mode of operation. Considering: $\frac{4}{e^{0.8} e^{\frac{q(V_{th} + \Delta\chi_{ms})}{1V}}} = A$ (from 116), the q_i from (110) is transformed into:

$$q_i = \text{Lambert}W \left[\frac{q t_{ox}}{\varepsilon_{ox}} \sqrt{\frac{n_i^2 \varepsilon_{si}}{2k_b T N_{si}}} \frac{e^{\frac{q(V_{ge} - \Delta\chi_{ms} - \phi_F)}{2k_b T}} e^{\frac{q(V_{ge} - V_{th} - \phi_F)}{2\eta_{eff} k_b T}}}{A + e^{\frac{q(V_{ge} - V_{th} - \phi_F)}{2\eta_{eff} k_b T}}} \right]$$

In addition, to model the I_{ds} , a flag $isSI$ is used, which is = 1 when the device is in strong inversion and = 0 when the device is in weak inversion. The $isSI$ function can be implemented by using ‘‘tanh’’ function [41–43], which is expressed as: $isSI = \frac{1}{2} + \frac{\tanh[\frac{5(V_g - \Delta V_{th})}{2}]}{2}$. Finally the I_{ds} model is expressed as:

$$I_{ds,SI} = \mu_n \left(\frac{2W}{L}\right) \left(\frac{2\varepsilon_{si}}{t_{si}}\right) \left(\frac{2k_b T}{q}\right)^2 \left[\left(\frac{q_{is}}{2r} - \frac{q_{id}}{2r}\right) + isSI \times r \left(\frac{q_{is}^2}{4r^2} - \frac{q_{id}^2}{4r^2}\right) \right]. \quad (117)$$

The complete I_{ds} model (118) is incorporated with various effects like surface roughness scattering, velocity saturation, series resistance between drain and source, and CLM (shown at the bottom of the page). where θ is the mobility attenuation factor due to surface roughness scattering, v_{sat} is the high-field electron drift-velocity saturation, R_{sd} is the equivalent resistance between the source and drain, and F_{CLM} is the CLM factor. For channel electric field of $E_y = 10^5 \text{ Vcm}^{-1}$ and higher, v_{sat} in the channel reaches a value about $v_{sat} = 10^7 \text{ cms}^{-1}$ [67]. The empirical relationship of F_{CLM} is:

$$F_{CLM} = 1 + \left(\frac{\lambda}{L}\right)^A \left(\frac{V_{ds,eff}}{V_{g,eff} - V_{th}}\right) \quad (119)$$

with $A = 1.2 - \sqrt{\lambda/L}$. In order to avoid a discontinuity at $V_g = V_{th}$ and $V_{ds} = V_g - V_{th}$, the smoothing functions: $V_{g,eff} = 2V_{th} + (V_g - 2V_{th}) \tanh(V_g/V_{th})^2$ and $V_{ds,eff} = V_{ds} \tanh(1.5V_{ds}/V_{g,eff})^2$ are introduced.

The I_{ds} models [22,23] are charge based compact model since the I_{ds} is expressed in terms of charge densities at source and drain ends. The short-channel models [20–23] have been integrated through Verilog-A code (given in Appendix A) in order to implement a DG MOSFET whose parameters are specified as: $L = 30 \text{ nm}$, $W = 50 \text{ nm}$, $t_{si} = 12 \text{ nm}$, $t_{ox} = 1 \text{ nm}$, $N_{si} = 10^{15} \text{ cm}^{-3}$, $N_{sd} = 10^{20} \text{ cm}^{-3}$, and $\mu_n = 500 \text{ cm}^2/\text{Vs}$. The Lambert W function has been coded using the algorithm given by Morris *et al.* [68]. Fig. 8 shows the I_{ds} characteristics observed in Spectre simulator for V_g sweep from 0 to 1.2 V at $V_{ds} = 1 \text{ V}$. Fig. 8(b) ensures symmetry of the device when the

$$I_{ds} = \frac{\mu_n}{1 + \theta(V_g - V_{th}) \left(1 + \frac{\mu_n V_{ds}}{v_{sat} L}\right) + \frac{2W C_{ox} \mu_n R_{sd} (V_g - V_{th})}{L}} \left(\frac{2W}{L}\right) \left(\frac{2\varepsilon_{si}}{t_{si}}\right) \left(\frac{2k_b T}{q}\right)^2 \left[(q_{is} - q_{id}) + isSI \times \frac{\varepsilon_{si} t_{ox}}{\varepsilon_{ox} t_{si}} (q_{is}^2 - q_{id}^2) \right] \times F_{CLM} \quad (118)$$

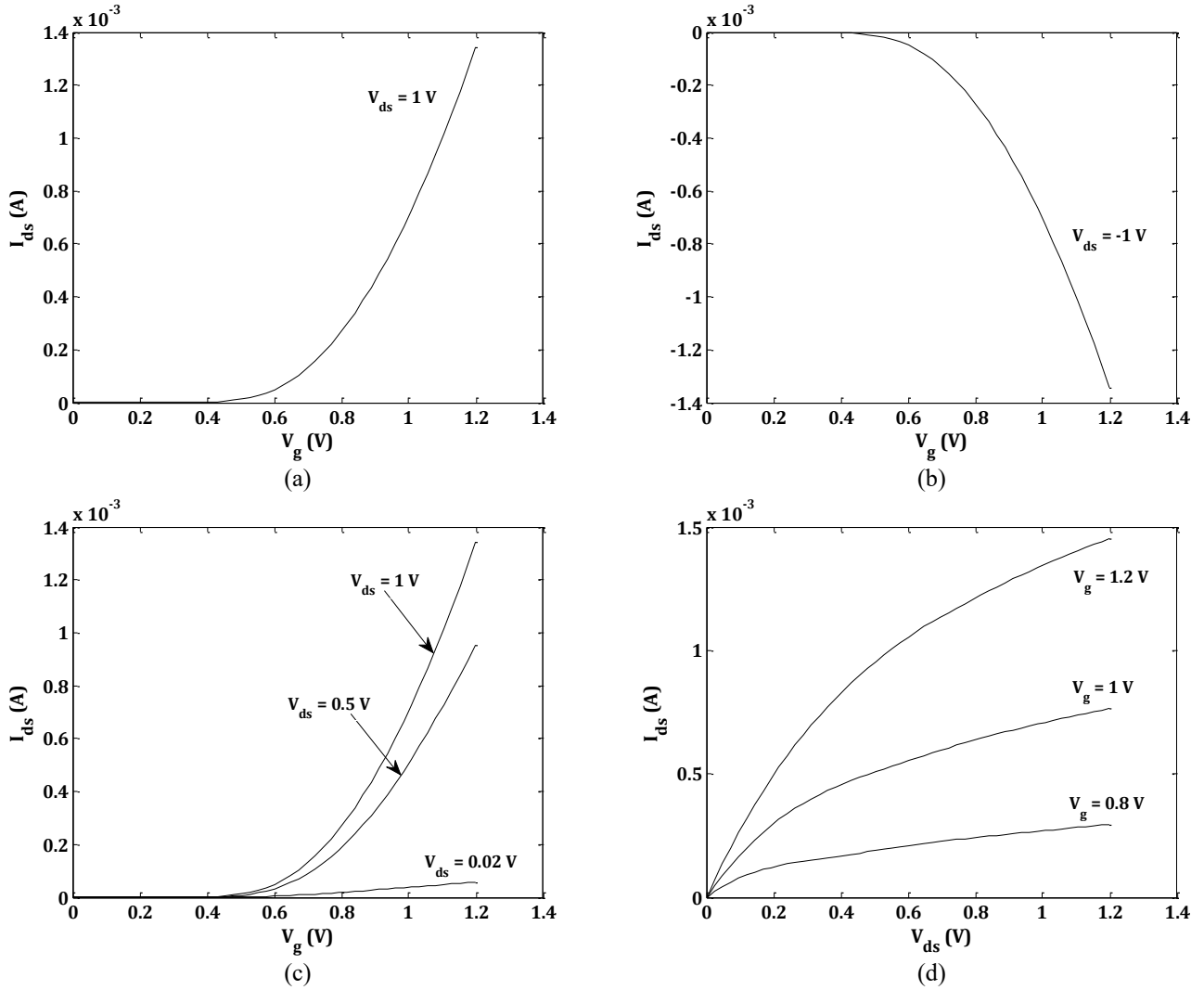


Fig. 8. Simulation results of short-channel DG MOSFET obtained in Spectre (a) transfer characteristics at $V_{ds}=1V$, (b) transfer characteristics at $V_{ds}=-1V$, (c) transfer characteristics for different values of V_{ds} , (d) output characteristics for different values of V_g .

polarity of V_{ds} is reversed. The transfer and output characteristics in Fig. 8 (c–d) are in close agreement with the simulation results in [23]. Fig. 9 shows the correlation between I_{ds} models (112) and (118); it is observed that the two different equations lead to similar results for the same DG MOSFET structure.

3) Taur et al. [24]:

This model is an improvement over the I_{ds} model [19] by considering the effect of lateral electric field on mobile charge density which was earlier ignored due to the assumption given by the GCA model. This model augments the GCA to produce finite output conductance in the saturation region. Addition to this, the conventional definition of pinch-off and CLM effects in the saturation region has been reinterpreted. Fig. 10 shows the comparison TCAD simulation results with the I_{ds} model [19] considering the parameters: $L = 100$ nm, $W = 1$ μ m, $t_{si} = 4$ nm, $t_{ox} = 2$ nm, $\epsilon_{si} = \epsilon_{ox} \approx 11.8\epsilon_0$, $\mu_n = 200$ cm²/(Vs), $N_{SD} = 10^{21}$ cm⁻³, and $V_0 = 0.33$ V. The TCAD simulation results [24] in Fig. 10 show that there is no

pinch-off point in the channel as depicted by GCA model. The failure of the GCA model in bulk MOSFETs was previously also demonstrated in [69] through the TCAD simulation. The pinch-off point is interpreted as the condition in the channel at which there is a sign change in the vertical electric field (E_x) occurs or $E_x = 0$, which has also been suggested earlier in [70] (for the bulk MOSFETs only). The CLM in saturation region is interpreted as the movement of the point at which the oxide electric field becomes zero in the source side. The complete I_{ds} model equation is expressed as:

$$\begin{aligned} \frac{I_{ds}}{\mu_n W} y = & \frac{4\epsilon_{si}}{t_{si}} \left(\frac{2k_b T}{q} \right)^2 \left[\beta \tan \beta - \frac{\beta^2}{2} + r\beta^2 \tan^2 \beta \right] \Big|_{\beta=\beta_d}^{\beta_s} \\ & - \frac{c_{ox}}{4} \left[|V_g - V_0 - V| - (V_g - V_0 - V) \right]^2 \\ & + \frac{\epsilon_{si} t_{si}}{2} \left[\left(\frac{dV}{dy} \right)^2 - E_0^2 \right], \end{aligned} \quad (120)$$

where E_0 is the lateral electric field at the source can be calculated numerically from the relation:

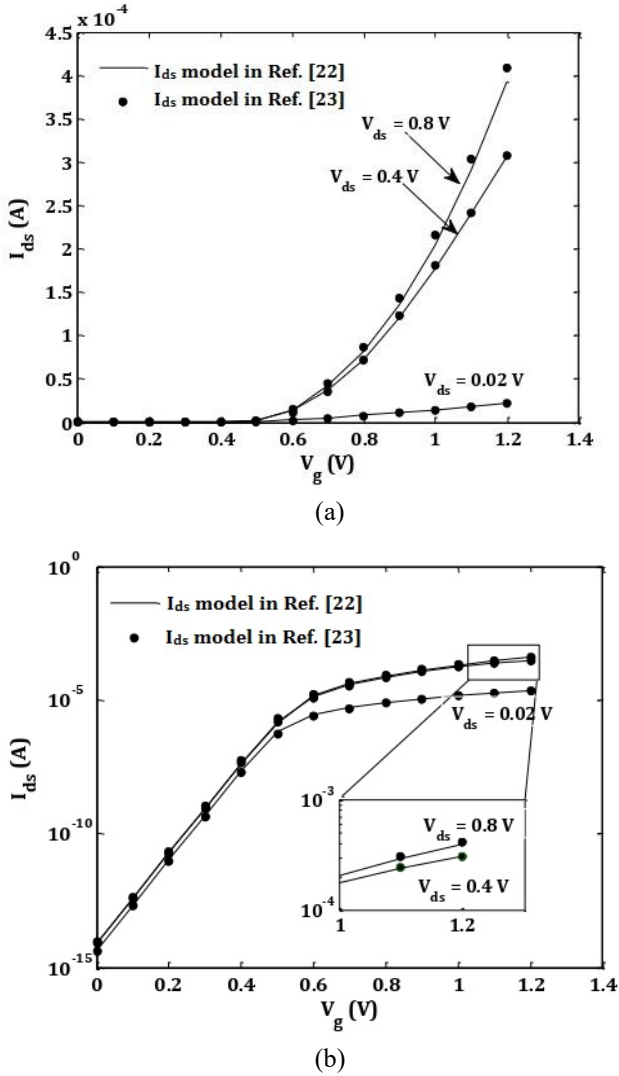


Fig. 9. Simulation results showing transfer characteristics of a short-channel DG MOSFET obtained from models (112) and (118) in (a) linear scale, (b) semi-logarithmic scale.

$$E_0 = \frac{I_{ds}}{2\mu_n W C_{ox}(V_g - V_0)} \quad (121)$$

The I_{ds} model (121) results are consistency with the TCAD simulation results.

IV. CONCLUSION

A comprehensive review based on the fundamental issues related to electrostatic potential, threshold voltage, and drain current formulations of analytic models for symmetric n-type DG MOSFETs for long as well as short channel have been presented in this paper. Equations for respective models have been analysed, and related derivations have been carried out for the further application of the models. Moreover, the correlation between the models carried out by various researchers has also been surveyed and discussed. This review provides an insight for understanding the mathematical models and also offers

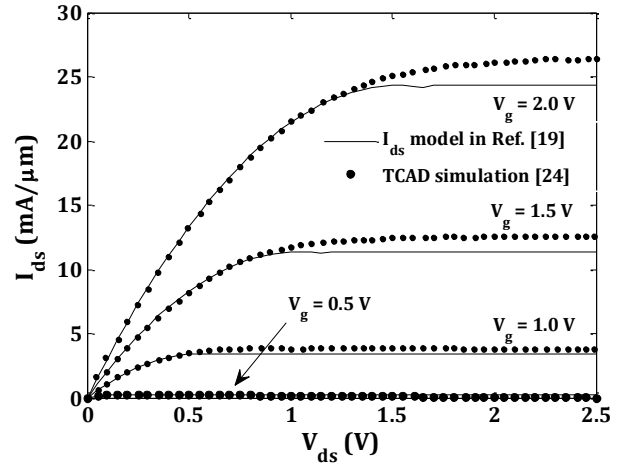


Fig. 10. Characteristics of a short-channel DG MOSFET obtained from model (93) in comparison with the TCAD simulation results [24].

knowledge for modeling and designing the increasingly important DG MOSFETs. This work can be of interest to researchers working in these MOSFETs.

APPENDIX

A. Verilog-A Implementation of Short-Channel DG MOSFET (n-Type)

```
// VerilogA for nDGMOS
`include "constants.vams"
`include "disciplines.vams"
module nDGMOS(Vgs,Vdd, Vss);
input Vgs;
inout Vdd, Vss;

// Technological Parameters
electrical Vgs, Vdd, Vss;
parameter real Eo=8.85e-12;
parameter real K=1.38e-23;
parameter real T=300;
parameter real q=1.6e-19;
parameter real tsi=12e-9;
parameter real tox=1e-9;
parameter real Nsi=1e21;
parameter real Nsd=1e26;
parameter real ni=1.45e16;
parameter real L=30e-9;
parameter real W=50e-9;
parameter real u=500e-4;
parameter real VT=0.0259;

// Model Parameters

real
Vg,Vd,Vs,Eox,Esi,lambda,Vfb,Vth,Vthlong,deltaVth,r
, fixed,power,n,nd,A,Vge,Vgeff,Vx,Vdeff,FCLM,num1
',
den1,qis,num2,den2,qid,isSI,x1,x2,SS;
```

```

// Threshold voltage calculation [ $V_{th}$  model(98)]:
analog function real threshold;
input l;
real
Eox, Esi, l, Vfb, Vbi, Vds, lambda, Qth, Q, den, k1, k2, k3;
begin
    Eox=3.9*Eo;
    Esi=11.68*Eo;

//Built-in potential:
    Vbi=VT*ln(Nsd*Nsi/pow(ni,2));
    Vds=0.02;

// Flat-band voltage:
    Vfb=-VT*ln(Nsi/ni);

// Natural channel length:
    lambda=sqrt(((Esi*tox*tsi)/(2*Eox))*(1+(Eox*tsi)/(4*Esi*tox)-(Eox*tsi)/(16*Esi*tox)));

// The  $Q_{th}$  (38):
    Qth=1e15*pow((1-(5+Vds)*(lambda/(2*l))),2);

    Q=(Qth*Nsi)/(pow(ni,2)*tsi);
    den=exp(1/lambda)-1;
    k1=(exp(4*l/lambda)-2*exp(2*l/lambda)+1)/pow(den,4);

    k2=(2*exp(1/(2*lambda))*(1+exp(1/lambda)))/pow(den,2);
    k3=(2*exp(3*l/lambda)-4*exp(2*l/lambda)+2*exp(1/lambda))/pow(den,4);

    threshold=Vfb+k1*VT*ln(Q)-k2*sqrt((Vbi-VT*ln(Q))*(Vbi+Vds-VT*ln(Q)))-k3*(2*Vbi+Vds);
end

endfunction

// Subthreshold slope calculation [20]:
analog function real subthreshold;
input l;
real Eox, Esi, l, lambda, alpha;
begin
    Eox=3.9*Eo;
    Esi=11.68*Eo;
    lambda=sqrt(((Esi*tox*tsi)/(2*Eox))*(1+(Eox*tsi)/(4*Esi*tox)-(Eox*tsi)/(16*Esi*tox)));
    alpha=L/(2*lambda);

    subthreshold=VT*ln(10)*((exp(4*alpha)-1)/(exp(4*alpha)+2*exp(alpha)-2*exp(3*alpha)));
end

endfunction

// lambertW function calculation [68]:
analog function real lambertw;
input x;
real
x, z, L1, L2, term1, term2, term3, term4, term5, term6, term7, term8, term9, term10, term11;

```

```

begin
    if(x<8)
    begin
        z=x/exp(1);
        term1=(z*(z-1))/(1+z);
        term2=(z*pow((z-1),2))/(2*pow((1+z),3));
        term3=(pow((z-1),3)*(z-2*pow(z,2)))/(6*pow((1+z),5));
        term4=(z*(6*pow(z,2)-8*z+1)*pow((z-1),4))/(24*pow((1+z),7));
        term5=(z*(24*pow(z,3)-58*pow(z,2)+22*z-1)*pow((z-1),5))/(120*pow((1+z),9));
        term6=(z*(120*pow(z,4)-444*pow(z,3)+328*pow(z,2)-52*z+1))/(720*pow((1+z),11));
        term7=(z*(720*pow(z,5)-3708*pow(z,4)+4400*pow(z,3)-1452*pow(z,2)+114*z-1))/(5040*pow((1+z),13));

        lambertw=z-term1+term2-term3+term4-term5+term6-term7;
    end

    else
    begin
        L1=ln(x);
        L2=ln(ln(x));
        term8=(L2*(-2+L2))/(2*pow(L1,2));
        term9=(L2*(6-9*L2+2*pow(L2,2)))/(6*pow(L1,3));
        term10=(L2*(-12+36*L2-22*pow(L2,2)+3*pow(L2,3)))/(12*pow(L1,4));
        term11=(L2*(60-300*L2+350*pow(L2,2)-125*pow(L2,3)+12*pow(L2,4)))/(60*pow(L1,5));

        lambertw=L1-L2+(L2/L1)+term8+term9+term10+term11;
    end

end

endfunction

//Drain-current calculation [23]:
analog begin
    Eox=3.9*Eo;
    Esi=11.68*Eo;
    Vg=V(Vgs);
    Vd=V(Vdd);
    Vs=V(Vss);
    Vfb=-VT*ln(Nsi/ni);
    lambda=sqrt(((Esi*tox*tsi)/(2*Eox))*(1+(Eox*tsi)/(4*Esi*tox)-(Eox*tsi)/(16*Esi*tox)));
    Vth=threshold(L);
    Vthlong=threshold(100e-9);
    delVth=Vth-Vthlong;
    r=(Esi*tox)/(Eox*tsi);
    fixed=((q*tox)/Eox)*sqrt((Esi*pow(ni,2))/(2*K*T*Nsi));
    power=1-sqrt(lambda/L);
    SS=subthreshold(L);
    n=SS/(VT*ln(10));
    nd=n/(2-n);
    A=(4/exp(0.8))*exp((Vth+Vfb)/1);
    Vge=Vg+delVth;
    Vgeff=2*Vth+(Vge-2*Vth)*tanh(pow((Vge/Vth),2));
    Vx=abs(Vd-Vs);

```

```

Vdeff=Vx*tanh(pow((1.5*Vx/Vgeff),2));
FCLM=1+(pow((lambda/L),power)*(Vdeff/(Vgeff-
Vth)));
num1=exp((Vg+delVth-Vfb-
Vs)/(2*VT))*exp((Vg+delVth-Vth-Vs)/(2*nd*VT));
den1=A+exp((Vg+delVth-Vth-Vs)/(2*nd*VT));
x1=fixed*num1/den1;

//Normalized charge density  $q_{is}$  and  $q_{id}$  [23]:
qis=lambertw(x1);
num2=exp((Vg+delVth-Vfb-
Vd)/(2*VT))*exp((Vg+delVth-Vth-Vd)/(2*nd*VT));
den2=A+exp((Vg+delVth-Vth-Vd)/(2*nd*VT));
x2=fixed*num2/den2;
qid=lambertw(x2);

//The  $i_{sI}$ :
isSI=(tanh(5*(Vg+delVth-Vth))/2)+0.5;

//The  $I_{ds}$  model (118):
I(Vdd,Vss)
<+((u*2*W/L)*(2*Esi/tsi)*pow((2*VT),2)*((qis/(2*
r))- (qid/(2*r))+isSI*r*(pow((qis/(2*r)),2)-
pow((qid/(2*r)),2))))*FCLM;
end
endmodule

```

ACKNOWLEDGMENT

The authors would like to thank Mr. Sheikh Wasmir Hussain, Research scholar from the Department of Electronics and Communication Engineering, National Institute of Technology Meghalaya, India for his help and useful suggestions.

REFERENCES

- [1] J. Koomey, S. Berard, M. Sanchez, and H. Wong, "Implications of historical trends in the electrical efficiency of computing," *IEEE Ann. Hist. Comput.*, vol. 33, no. 3, pp. 46-54, Mar. 2011.
- [2] H.R. Huff, "John Bardeen and transistor physics," in *Proc. AIP Conf.*, vol. 550, no. 3, pp. 3-29, Mar. 2001.
- [3] W.C. Holton and R.K. Cavin, "A Perspective on CMOS technology trends," in *Proc. IEEE*, vol. 74, no. 12, pp. 1646-1668, Dec. 1986.
- [4] D. Kahng, "A historical perspective on the development of MOS transistors and related devices," *IEEE Trans. Electron Devices*, vol. 23, no. 7, pp. 655-657, Jul. 1976.
- [5] F. Wanlass and C. Sah, "Nanowatt logic using field-effect metal-oxide semiconductor triodes," in *Proc. IEEE Solid-State Circuits Conf.*, vol. 6, pp.32-33, Feb. 1963.
- [6] D.J. Frank *et al.*, "Device scaling limits of Si MOSFETs and their application dependencies," in *Proc. IEEE*, vol. 89, no. 3, pp. 259-288, Mar. 2001.
- [7] N. Z. Haron and S. Hamdioui, "Why is CMOS scaling coming to an END?," in *Proc. 3rd Int. Design Test Workshop*, Dec. 2008, pp. 98-103.
- [8] A. Asenov *et al.*, "Increase in the random dopant induced threshold fluctuations and lowering in sub-100 nm MOSFETs due to quantum effects: a 3-D density gradient simulation study," *IEEE Trans. Electron Devices*, vol. 48, no. 4, pp. 722-729, Apr. 2001.
- [9] R.-H. Yan, A. Ourmazd, and K.F. Lee, "Scaling the Si MOSFET: from bulk to SOI to bulk," *IEEE Trans. Electron Devices*, vol. 39, no. 7, pp. 1704-1710, Jul. 1992.
- [10] Q. Xie, J. Xu, and Y. Taur, "Review and critique of analytic models of MOSFET short-channel effects in subthreshold," *IEEE Trans. Electron Devices*, vol. 59, no. 6, Jun. 2012.
- [11] I. Ferain, C.A. Colinge, and J.-P. Colinge, "Multigate transistors as the future of classical metal-oxide-semiconductor field-effect-transistor," *Nature*, vol. 479, no. 7373, pp. 310-316, Nov. 2011.
- [12] T. Sekigawa and Y. Hayashi, "Calculated threshold-voltage characteristics of an X MOS transistor having an additional bottom gate," *Solid-State Electron.*, vol. 27, no. 8-9, pp. 827-828, Aug. 1984.
- [13] H. Lu, "Compact modeling of double-gate MOSFETs," Ph.D dissertation, Univ. California, San-Diego, CA, 2006.
- [14] F. Balestra *et al.*, "Double-gate silicon-on-insulator transistor with volume inversion," *IEEE Electron Device Lett.*, vol. 8, no. 9, pp. 410-412, Sep. 1987.
- [15] Y. Taur, "An analytical solution to a double-gate MOSFET with undoped body," *IEEE Electron Device Lett.*, vol. 21, no. 5, pp. 245-247, May, 2000.
- [16] H. Lu and Y. Taur, "An analytic potential model for symmetric and asymmetric DG MOSFETs," *IEEE Trans. Electron Devices*, vol. 53, no. 5, pp. 1161-1168, May 2006.
- [17] C. Hong, J. Zhou, Q. Cheng, K. Zhu, J.B. Kio, and Y. Chen, "Unified continuous and discrete model for double-gate MOSFETs with spatially varying or pulsed doping profiles," *IEEE J. Electron Devices Soc.*, vol. 5, no. 4, pp. 244-255, Jul. 2017.
- [18] Q. Chen, E.M. Harrell and J.D. Meindl, "A physical short-channel threshold voltage model for undoped symmetric double-gate MOSFETs," *IEEE Trans. Electron Devices*, vol. 50, no. 7, pp. 1631-1637, Jul. 2003.
- [19] Y. Taur, X. Liang, W. Wang, and H. Lu, "A continuous, analytic drain-current model for DG MOSFETs," *IEEE Electron Device Lett.*, vol. 25, no. 2, pp. 107-109, Feb. 2004.
- [20] A. Tsormpatzoglou *et al.*, "Semi-analytical modeling of short-channel effects in Si and Ge symmetrical double-gate MOSFETs," *IEEE Trans. Electron Devices*, vol. 54, no. 8, pp. 1943-1952, Aug. 2007.
- [21] A. Tsormpatzoglou *et al.*, "Threshold voltage model for short-channel undoped symmetrical double-gate MOSFETs," *IEEE Trans. Electron Devices*, vol. 55, no. 9, pp. 2512-2516, Sep. 2008.
- [22] A. Tsormpatzoglou *et al.*, "Analytical modelling for the current-voltage characteristics of undoped or lightly-doped symmetric double-gate MOSFETs," *Microelectron. Eng.*, vol. 87, no. 9, pp. 1764-1768, Nov. 2010.
- [23] K. Papathanasiou *et al.*, "Symmetrical unified compact model for short-channel double-gate MOSFETs," *Solid-State Electron.*, vol. 69, pp. 55-61, Mar. 2012.
- [24] Y. Taur and H.-H. Lin, "Modeling of DG MOSFET $I - V$ characteristics in the saturation region," *IEEE Trans. Electron Devices*, vol. 65, no. 5, pp. 1714-1720, May 2018.
- [25] B. Yu, H. Lu, M. Liu, and Y. Taur, "Explicit continuous models for double-gate and surrounding-gate MOSFETs," *IEEE Trans. Electron Devices*, vol. 53, no. 10, pp. 2715-2721, Oct. 2007.
- [26] V.R. Mural and C. Vijaya, "A quasi-ballistic drain current, charge and capacitance model with positional carrier scattering dependency valid for symmetric DG MOSFETs in nanoscale regime," *Nano Convergence*, vol. 6, no. 19, Jun. 2019.
- [27] J.-M. Sallese, F. Krummenacher, F. Pregaldiny, C. Lallement, A. Roy, and C. Enz, "A design oriented charge-based current model for symmetric DG MOSFET and its correlation with the EKV formalism," *Solid-State Electron.*, vol. 49, no. 3, pp. 485-489, Mar. 2005.
- [28] V. Hariharan, J. Vasi, and V.R. Rao, "Drain current model including velocity saturation for symmetric double-gate MOSFETs," *IEEE Trans. Electron Devices*, vol. 55, no. 8, pp. 2173- 2180, Aug. 2008.
- [29] L. Zhang, Y. Guan, W. Zhou, L. Chen, Y. Xu, and J. He, "A carrier-based analytic drain current model incorporating velocity saturation for undoped surrounding-gate MOSFETs," *Semicond. Sci. Technol.*, vol. 24, no. 11, pp. 115003, Oct. 2009.
- [30] Z. Chen *et al.*, "Surface-potential based drain current model for long channel junctionless double-gate MOSFETs," *IEEE Trans. Electron Devices*, vol. 59, no. 12, pp. 3292-3298, Dec. 2012.
- [31] X. Jin, X. Liu, M. Wu, R. Chuai, and J.-H. Lee, and J.-H. Lee, "A unified analytical continuous current model applicable to accumulation mode (junctionless) and inversion mode MOSFETs with symmetric and

- asymmetric double-gate structures," *Solid-State Electron.*, vol. 79, pp. 206-209, Jan. 2013.
- [32] V.K.S. Yadav and R.K. Baruah, "An analytic potential and threshold voltage model of short-channel symmetric double-gate MOSFET," in *Proc. IEEE Int. Symp. VLSI Design Test*, Jul. 2014.
- [33] H.A.E. Hamid, J. R. Guitart, and B. Iniguez, "Two-dimensional analytical threshold voltage and subthreshold swing models of undoped symmetric double-gate MOSFETs," *IEEE Trans. Electron Devices*, vol. 54, no. 6, pp. 1402-1408, Jun. 2007.
- [34] B. Ray and S. Mahapatra, "Modeling of channel potential and subthreshold slope of symmetric double-gate transistor," *IEEE Trans. Electron Devices*, vol. 56, no. 2, pp. 260-266, Feb. 2009.
- [35] S.-H. Oh, D. Monroe, and J.M. Hergenrother, "Analytic description of short-channel effects in fully depleted double-gate and cylindrical surrounding-gate MOSFETs," *IEEE Electron Device Lett.*, vol. 21, no. 9, pp. 445-447, Nov. 2000.
- [36] F. Lime, B. Iniguez, and O. Moldovan, "A quasi-two-dimensional compact drain-current model for undoped symmetric double-gate MOSFETs including short-channel effects," *IEEE Trans. Electron Devices*, vol. 55, no. 6, pp. 1441-1448, Jun. 2008.
- [37] H. Abebe *et al.*, "Symmetric and asymmetric double gate MOSFET modelling," *J. Semicond. Technol. Sci.*, vol. 9, no. 4, pp. 225-232, Dec. 2009.
- [38] J. Prasad, A. Agarwal, P.C. Pradhan, and B.P. Swain, "Analytical modeling of surface potential for double-gate MOSFET," in *Advances in Communication, Devices and Networking. Lecture Notes in Electrical Engineering*, vol. 537. R. Bera, S. Sarkar, O. Singh, and H. Saikia, Eds. Singapore: Springer, 2019, pp. 55-62.
- [39] X. Liang and Y. Taur, "A 2-D analytical solution for SCEs in DG MOSFETs," *IEEE Trans. Electron Devices*, vol. 51, no. 8, pp. 1385-1391, Aug. 2004.
- [40] N. Pandey, H.-H. Lin, A. Nandi, and Y. Taur, "Modeling of short-channel effects in DG MOSFETs: Green's function method versus scale length model," *IEEE Trans. Electron Devices*, vol. 65, no. 8, pp. 3112-3119, Aug. 2018.
- [41] A. Cerdeira, B. Iniguez, and M. Estrada, "Compact model for short channel symmetric doped double-gate MOSFETs," *Solid-State Electron.*, vol. 52, no. 7, pp. 1064-1070, Jul. 2008.
- [42] A. Cerdeira, O. Moldovan, B. Iniguez, and M. Estrada, "Modeling of potentials and threshold voltage for symmetric doped double-gate MOSFETs," *Solid-State Electron.*, vol. 52, no. 5, pp. 830-837, May 2008.
- [43] J. Alvarado *et al.*, "Implementation of the symmetric double-gate MOSFET model in Verilog-A for circuit simulation," *Int. J. Numer. Model., Electron, Netw, Devices Fields*, vol. 23, no. 2, pp. 88-106, Mar/Apr. 2010.
- [44] M. Cheralathan *et al.*, "Compact drain-current model for reproducing transport advanced transport models in nanoscale double-gate MOSFETs," *Semicond. Sci. Technol.*, vol. 26, no. 9, pp. 095015, Jul. 2011.
- [45] M. Cheralathan *et al.*, "Implementation of nanoscale double-gate CMOS circuits using compact advanced transport models," *Microelectronics J.*, vol. 44, no. 2, pp. 80-85, Feb. 2013.
- [46] A. Qrtiz-Conde, F.J. Garcia-Sanchez, J. Muci, S. Malobabic, and J.J. Liou., "A review of core compact models for undoped double-gate SOI MOSFETs," *IEEE Trans. Electron Devices*, vol. 54, no. 1, pp. 131-140, Jan. 2007.
- [47] J. Song, B. Yu, Y. Yuan, and Y. Taur, "A review on compact modeling of multiple-gate MOSFETs," *IEEE Trans. Circuits Syst.-I: Reg. Papers*, vol. 54, no. 1, pp. 1858-1869, Jul. 2009.
- [48] K.K. Young, "Short-channel effect in fully depleted SOI MOSFETs," *IEEE Trans. Electron Devices*, vol. 36, no. 2, pp. 399-402, Feb. 1989.
- [49] Verilog-A language reference manual: analog extensions to Verilog HDL, version 1.0, Open Verilog International; 1996.
- [50] H.C. Pao and C.T. Sah, "Effects of diffusion current on characteristics of metal-oxide (insulator)-semiconductor transistors," *Solid-State Electron.*, vol. 9, no. 10, pp. 927-937, Oct. 1966.
- [51] Y. Taur and T. Ning, *Fundamentals of VLSI Devices*. Cambridge, U.K.: Cambridge Univ. Press, 2009.
- [52] J.R. Hauser and M.A. Littlejohn, "Approximations for accumulation and inversion space-charge layers in semiconductor," *Solid-State Electron.*, vol. 11, no. 7, pp. 667-674, Jul. 1968.
- [53] R.U. Ahmed and P. Saha, "Modeling of threshold voltage and subthreshold current for p-channel symmetric double-gate MOSFET in nanoscale regime," in *Proc. IEEE Int. Symp. Nanoelectron. Information Syst.*, Dec. 2017, pp. 179-183.
- [54] B.S. Grewal, *Higher Engineering Mathematics*. New Delhi, India: Khanna Publishers, 2012.
- [55] R. Shankar, G. Kaushal, S. Maheshwaram, S. Dasgupta, and S.K. Manhas, "A degradation model of double-gate and gate-all-around MOSFETs with interface trapped charges including effects of channel mobile charge carriers," *IEEE Trans. Device Material Reliab.*, vol. 14, no. 2, pp. 689-697, Jun. 2014.
- [56] J. Zhou, "On compact model for double-surrounding-gate MOSFETs and the yield study of lithographic processes," Ph.D dissertation, Peking Univ., Beijing, China, 2016.
- [57] J.R. Brews, "A charge-sheet model of the MOSFET," *Solid-State Electron.*, vol. 21, no. 2, pp. 345-355, Feb. 1978.
- [58] A. Dasgupta, A. Agarwal S. Khandelwal, and Y.S. Chauhan, "Compact modeling of surface potential, charge, and current in nanoscale transistors under quasi-ballistic regime," *IEEE Trans. Electron Devices*, vol. 63, no. 11, pp. 4151-4159, Nov. 2016.
- [59] M. Reyboz, O. Rozeau, and T. Poiroux, "Compact modeling of double gate MOSFET for IC design," in *Planar Double-Gate Transistor. From Technology to Circuit*. A. Amara and O. Rozeau, Eds. Dordrecht: Springer, 2009, pp. 55-88.
- [60] D. M. Caughey and R. E. Thomas, "Carrier mobilities in silicon empirically related to doping and field," *Proc. IEEE*, vol. 55, no. 12, pp. 2192-2193, Dec. 1967.
- [61] C. Lombardi, S. Manzini, A. Saporito, and M. Vanzi, "A physically based mobility model for numerical simulation of nonplanar devices," *IEEE Trans. Comput.-Aided Des.*, vol. 7, no. 11, pp. 1164-1171, Nov. 1988.
- [62] N. Arora, *MOSFET Models for VLSI Circuit Simulation: Theory and Practice*. New York, USA: Springer-Verlag, 1993.
- [63] R.K. Baruah and S. Mahapatra, "Justifying threshold voltage definition for undoped body transistors through 'crossover point' concept," *Physica B*, vol. 404, no. 8-11, pp. 1029-1032, May 2009.
- [64] D. J. Frank, Y. Taur, and H.-S. P. Wong, "Generalized scale length for two-dimensional effects in MOSFETs," *IEEE Electron Device Lett.*, vol. 19, no. 10, pp. 385-387, Oct. 1998.
- [65] A. Nandi, N. Pandey, and S. Dasgupta, "Analytical modeling of DGMOSFET in subthreshold regime by green's function approach," *IEEE Trans. Electron Devices*, vol. 64, no. 8, pp. 3056-3062, Aug. 2017.
- [66] A. Ortiz-Conde, F.J. Garcia-Sanchez, and M. Guzman, "Exact analytical solution of channel surface potential as an explicit function of gate voltage in undoped-body MOSFETs using the LambertW function and a threshold voltage therefrom," *Solid-State Electron.*, vol. 47, no. 11, pp. 2067-2074, Nov. 2003.
- [67] S.-M. Kang and Y. Leblebici, *CMOS Digital Integrated Circuits Analysis and Design*. New York, USA: Mc-Graw Hill, 2003.
- [68] H. Morris, E. Cumberbatch, H. Abebe, and V. Tyree, "Compact models for the I-V characteristics of double-gate and surround gate MOSFETs," in *Proc. IEEE UGIM Symp.*, Jun. 2006, pp. 119-123.
- [69] X. Yang and D. K. Schroder, "Some semiconductor device physics considerations and clarifications," *IEEE Trans. Electron Devices*, vol. 59, no. 7, pp. 1993-1996, Jul. 2012.
- [70] Y. Tsidividis, *Operation and Modeling of the MOS Transistor*. New York, NY, USA: McGraw-Hill, 1999.